Mapping the Climate of Puerto Rico, Vieques and Culebra

CHRISTOPHER DALY, [1*] E. H. HELMER, [2] AND MAYA QUIÑONES [2]

[1]*Spatial Climate Analysis Service, Department of Geosciences, 316 Strand Agricultural Hall, Oregon State University, Corvallis, OR 97331-2204, USA*

[2]*International Institute of Tropical Forestry, USDA Forest Service, P.O. Box 25000, Río Piedras, 00928-5000, Puerto Rico*

ABSTRACT

Spatially explicit climate data contribute to watershed resource management, mapping vegetation type with satellite imagery, mapping present and hypothetical future ecological zones, and predicting species distributions. The regression based Parameter-elevation Regressions on Independent Slopes Model (PRISM) uses spatial data sets, a knowledge base and expert interaction to generate GIS-compatible grids of climate variables. This study applied PRISM to generate maps of mean monthly and annual precipitation and minimum and maximum temperature for the Caribbean islands of Puerto Rico, Vieques and Culebra over the 1963-1995 averaging period. PRISM was run under alternative parameterizations that simulated simpler interpolation methods as well as the full PRISM model. For temperature, the standard PRISM parameterization was compared to a hypsometric method, in which the temperature/elevation slope was assumed to be -6.5°C/km (HYPS). For precipitation, the standard PRISM parameterization was compared to an inverse-distance weighting interpolation (IDW). Spatial temperature patterns were linked closely to elevation, topographic position, and coastal proximity. Both PRISM and HYPS performed well for July maximum temperature, but HYPS performed relatively poorly for January minimum temperature, due primarily to lack of a spatially varying temperature/elevation slope, vertical atmospheric layer definition, and coastal proximity guidance. Mean monthly precipitation varied significantly throughout the year, reflecting seasonally differing moisture trajectories. Spatial precipitation patterns were associated most strongly with elevation, upslope exposure to predominant moisture-bearing winds, and proximity to the ocean. IDW performed poorly compared to PRISM, due largely to the lack of elevation and moisture availability information. Overall, the full PRISM approach resulted in greatly improved performance over simpler methods for precipitation and January minimum temperature, but only a small improvement for July maximum temperature. Comparisons of PRISM mean annual temperature and precipitation maps to previously-published, hand-drawn maps showed similar overall patterns and magnitudes, but the PRISM maps provided much more spatial detail.

Correspondence to: Christopher Daly, Spatial Climate Analysis Service, Department of Geosciences, 326 Strand Agriculture Hall, Oregon State University, Corvallis OR 97331-2204, USA; email: daly@coas.oregonstate.edu

1. INTRODUCTION

Many spatially explicit ecological and hydrological models require spatially continuous climate data. As scientists and managers using these models work at finer spatial and temporal resolution, higher resolution climate data become more relevant. In the tropics and elsewhere, spatially continuous climate data help predict woody vegetation (Ohmann and Spies, 1998, Foster *et al*., 1998, Bongers, 1999, Ohmann and Gregory, 2002) and vertebrate species distributions (Woinarski *et al*., 1999, Joseph and Stockwell, 2000, Stockwell and Peters, 1999). Seasonal variability and climate extremes can be more important to distributions of woody plant species than annual means (Ohmann and Spies, 1998), which illustrates the importance of climate data with temporal resolution finer than annual. Many spatially explicit terrestrial ecosystem models, like those that predict vegetation primary production and related parameters, also rely on climate data, including at daily resolution (e.g. Running and Gower, 1991, Running and Hunt, 1993). These models can also use monthly climate data (Tian *et al*., 2000, Wang *et al*., 2001), and include examples of predicting nitrogen trace gas emissions from soils (Liu *et al*., 2000).

Climate data have long been important to mapping potential vegetation or ecological zones (Holdridge *et al*., 1971, Ewel and Whitmore, 1973), and such mapping has become more sophisticated or increased in spatial resolution recently (Neilson, 1995, Host *et al*., 1996, Lugo *et al*., 2000, Isaac and Bourque, 2001). Ecological zone maps or spatially continuous climate data can also be important for mapping vegetation type with satellite imagery (e.g. He *et al*., 1998). Such data are crucial to satellite image based mapping of land cover, vegetation type or forest successional stage in complex tropical areas (Helmer *et al*., 2000, Helmer *et al*., 2002). Ecological zones and illumination angles change rapidly in such regions, which leads to spectral confusion in which varied vegetation communities have similar spectral signatures. In addition, the ranges of forest successional stages produced by human disturbance compound spectral confusion between vegetation types. Puerto Rico, which is the focus of this study, is an especially complex Caribbean island. In the Caribbean, ecological zones change rapidly over small areas due to complex topography, climate and soils (Beard, 1949). Conservation of the many endemic species found in these complex tropical islands requires maps with finer spatial and class resolution than existing global- or sub continental-scale ecological zone or satellite image based maps provide (Helmer *et al*., 2002).

Furthermore, efficient water resource management is critical to Caribbean islands. Periodic droughts in Caribbean islands cause economic losses and hardships because high population densities combine with limited water resources and storage capacity (Granger, 1983, Larsen, 2001). Spatially continuous data on climate and watershed characteristics improve accuracy of water discharge predictions in Puerto Rico and elsewhere (García-Martinó *et al*., 1996a), which should contribute to water resources management. Developing spatially continuous rainfall data, for example, contributed to estimating low stream flow in Northeastern Puerto Rico (García-Martinó *et al*., 1996a, b). Rainfall is also related to erosion, so spatially explicit models that simulate erosion under various land use configurations (López *et al*., 1998) can point towards landscape management that minimizes sedimentation flow to reservoirs. Finally, biogeographical and other modeling that relies on climate data can predict potential patterns of change in vegetation

and runoff induced by climate change (Nelson and Marks, 1994, Iverson and Prasad, 1998). These modeling efforts are especially important for Caribbean islands, where vegetation and water resources may be particularly vulnerable to global climate change. Scatena (1998) predicted that increases in coastal plain temperature of 1 to 2° C, or decreases in rainfall of 11 to 33%, would adversely impact water supplies, as well as impact the distribution of forest types in the Luquillo Mountains of Puerto Rico, potentially affecting endemic species.

To support mapping and spatially explicit analysis of vegetation composition, structure and other attributes, species distributions, ecosystem modeling, and water resources management in Puerto Rico, we had the objective of mapping annual and monthly rainfall and temperature at a relatively fine spatial resolution. The Parameter-elevation Regressions on Independent Slopes Model (PRISM) (Daly and Neilson, 1992, Daly et al., 1994, 1997, in press) is especially suited to mapping climate in a complex landscape like that of Puerto Rico. This study describes application of PRISM to the particular landscapes of Puerto Rico, Vieques and Culebra, under alternative parameterizations that simulate simpler interpolation methods as well as the full PRISM model. The effectiveness of each method is assessed, and compared and contrasted with other methods. All simulations are made at 15 arc-seconds (~450 m) as a spatial resolution that would capture the island's complexity and improve on current data for satellite image based mapping.

The regression-based PRISM uses point data, a digital elevation model (DEM), other spatial data sets, a knowledge base, and expert interaction to generate repeatable estimates of annual, monthly, daily, and event-based climatic elements. These estimates are interpolated to a regular grid, making them GIS-compatible. Recent mapping efforts include peer-reviewed, official USDA precipitation and temperature maps for all 50 states and Pacific Islands (Bishop et al., 1998, USDA-NRCS, 1998, Daly and Johnson, 1999, Vogel et al., 1999, Daly et al., 2001); a new official climate atlas for the United States (Plantico et al., 2000); a 103-year series of monthly temperature and precipitation maps for the conterminous 48 states (Daly et al., 2000b); precipitation and temperature maps for Canada, China and Mongolia (Daly et al., 2000a), and the first comprehensive precipitation maps for the European Alps region (Schwarb et al., 2001a, 2001b).

2. METHODS

2.1. Study Area

The main island of Puerto Rico lies between about 17°45' N and 18°30' N, and its longitude ranges from about 65°45' W to 67°15' W (Figure 1). With the main island occupying about 8740 km^2, it is the smallest and easternmost of the Greater Antilles. Vieques and Culebra Islands lie a short distance to the east of the main island, with areas of 125 km^2 and 25 km^2, respectively. Vieques and Culebra are the westernmost of the Lesser Antilles, which extend in a southeasterly arc from Puerto Rico to the northern coast of South America. Vegetation zones on the main island range from dry, semi deciduous forests in patches and bands on the north and east coasts and in the southwest part of the island, to moist forests that cover the major proportion of the island, to wet and rain forests, including cloud forests, at higher elevations. Elevations range from sea level to 1338 m at Cerro de Punta, in the Cordillera Central on the main island (Figure 1).

Puerto Rico, Vieques, and Culebra have a climate that is tropical and predominantly maritime, typical of the Caribbean islands. Temperatures exhibit small seasonal variation, due to close proximity to the equator. Temperatures at sea level are quite warm, but decrease markedly with increasing elevation. Humidity is generally high, due to the presence of warm ocean waters. Rainfall and cloudiness are influenced strongly by topography, with mountainous regions being much cloudier and wetter than adjacent lowlands and ocean areas. During May to November, precipitation is produced mainly by easterly waves, which are disturbances embedded in the generally east-to-west trade winds across the region. The strength of these waves ranges greatly, from low-intensity systems accompanied by little or no rainfall, to intense systems that produce flooding rains. The greatest rainfall occurs when tropical storms or hurricanes occasionally develop on these waves and move across or near Puerto Rico. During November to April, cold fronts moving off the eastern US seaboard, that penetrate far enough south to affect the islands, can produce significant precipitation.

2.2. Climate Data

Monthly average minimum (T_{min}) and maximum (T_{max}) temperatures for the years 1963 -1995 were calculated for 47 National Weather Service cooperative stations using daily data from the National Climate Data Center (NCDC 1995) (Figure 1). Monthly and annual average T_{min} and T_{max} over the period were derived from averaging monthly and yearly data over all years, ignoring missing data. Three estimated minimum temperature sites were added in the vicinity of Adjuntas to aid in the spatial definition of a local nighttime temperature minimum in this area. Estimates were made based on an analysis of likely topographic constraints to cold air drainage. Mean monthly and annual precipitation totals were calculated for the period 1963-1995 using monthly data for 108 stations from the NCDC. Additional precipitation data were obtained from a station at El Verde, in the Luquillo Mountains. This station, operated by the University of Puerto Rico, had 19 years of record (Garcia-Martino *et al*., 1996a).
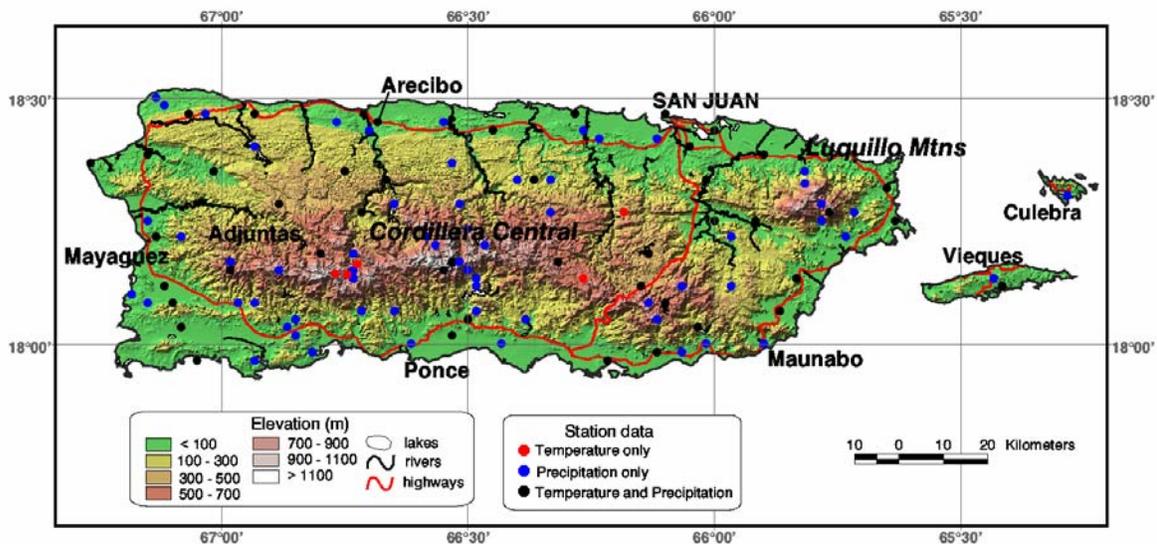

Figure 1: Terrain map of Puerto Rico, Vieques, and Culebra, showing climate station locations

2.3. PRISM Model Formulation for Climate Mapping

  PRISM adopts the assumption that for a localized region, elevation is the most important factor in the distribution of temperature and precipitation (Daly *et al*., 2002). PRISM calculates a linear climate-elevation relationship for each DEM grid cell, but the slope of this line changes locally with elevation as dictated by the data points. Beyond the lowest or highest station, the function can be extrapolated linearly as far as needed. A simple, rather than multiple, regression model was chosen because controlling and interpreting the complex relationships between multiple independent variables and climate is difficult. Instead, weighting the data points (discussed later) controls the effects of variables other than elevation.

  The climate-elevation regression is developed from x,y pairs of elevation and climate observations supplied by station data. A moving-window procedure is used to calculate a unique climate-elevation regression function for each grid cell. The simple linear regression has the form

(1) $$Y = \beta_1 X + \beta_0$$

where Y is the predicted climate element, β_1 and β_0 are the regression slope and intercept, respectively, and X is the DEM elevation at the target grid cell. The DEM elevation is expressed at a scale appropriate for the climate element being mapped (see Section 2.3.1).

  Upon entering the regression function, each station is assigned a weight that is based on several factors. In the general PRISM formulation, the combined weight of a station is a function of distance, elevation, cluster, vertical layer, topographic facet, coastal proximity, and effective terrain weights, respectively. A full discussion of the station weighting functions is available in Daly (2002) and Daly et al. (2002). A subset of these functions was used for Puerto Rico. For modeling in the present study area, the combined weight W of a station was a function of the following:

(2) $$W = f\{ W_d, W_z, W_c, W_p, W_l, W_e \}$$

where W_d, W_z, W_c, W_p and W_e are the distance, elevation, cluster, coastal proximity, vertical layer, and effective terrain weights, respectively. Distance, elevation, and cluster weighting are relatively straightforward in concept. A station is down-weighted when it is relatively distant or at a much different elevation than the target grid cell, or when it is clustered with other stations (which leads to over-representation). Coastal proximity weighting is used to define gradients in precipitation or temperature that may occur due to proximity to large water bodies (Daly *et al*., 1997, Daly and Johnson, 1999, Daly *et al*., 2002). Vertical layer weighting is used to simulate situations where rapid changes, or even reversals, in the relationship between climate and elevation are possible (i.e., temperature inversions). When the potential for such situations exists, the climate stations entering the regression are divided into two vertical layers, and regressions run on each separately. Layer 1 represents the boundary layer, and layer 2 represents the free atmosphere above it. Effective terrain weighting accounts for differences in the ability of terrain features to enhance precipitation through mechanical uplift of moisture-bearing air. Features having relatively steep, bulky profiles typically produce strong precipitation-

elevation relationships; while low, gently rolling features have weaker relationships (Daly *et al*., 1997, Daly and Johnson, 1999, Daly, 2002).

2.3.1. Elevation Data

All climate elements were interpolated to a regular grid with a resolution of 15 seconds (~450 m) (Figure 1). DEMs of Puerto Rico, Vieques, and Culebra with a grid cell resolution of 3 seconds (~90 m), 1 second (30 m) and 1 second (30 m), respectively, were obtained from the U.S. Geologic Survey, and filtered to15-second resolution with a modified Barnes filter (Barnes, 1964). The temperature mapping procedure used this 15-second DEM as the elevation grid. For precipitation mapping, the modified Barnes filter was used to smooth the DEM to an effective wavelength of 2.5 minutes (~ 4.5 km), while maintaining the 15-second resolution, effectively removing small-wavelength features from the grid. Previous studies have shown that precipitation patterns are more highly correlated with broad-scale topographic features than with local features (e.g., Spreen, 1947, Burns, 1953, Schermerhorn, 1967, Daly *et al*., 1994, Kyriakidis *et al*., 2001). Many of these studies and results from other PRISM modeling activities suggest that 2.5 minutes is near the optimum resolution for modeling precipitation.

2.3.2. Coastal Proximity Guidance – Coastal Advection Model

Preliminary analysis of the temperature data with the PRISM graphical user interface (Daly *et al*., 2002) revealed that there were significant coastal influences on the spatial patterns of temperature. Therefore, a simple coastal advection model designed for PRISM was used to quantify coastal proximity for temperature mapping. The advection model is a cost-benefit algorithm that assesses the optimal path a surface air parcel might take as it moves from the coast to each inland pixel. The basic assumption is that the mean coastal influence experienced at a site will be the result of a flow path from the coast that minimizes two factors: (1) modification of the air by continental influences, which accumulates as the path length over land increases (hereafter called the coastal path length penalty); and (2) loss of momentum caused by flowing over terrain obstacles (hereafter called the terrain penalty). Predominant mesoscale flow patterns, which will aid certain flow paths and cause more effective inland penetration, are also accounted for.

To begin the simulation, ocean pixels along the coastline were assigned a "coastal influence" (CI) score of 0. The unfiltered, 15-second DEM was used to describe the terrain. As a first guess, the shortest paths between each land pixel and the coastline were chosen as the preferred paths and the CI scores assessed. The CI score at pixel n was calculated as follows:

(3) $$CI_n = CI_{n-1} + 0.5((t_{up} + t_{down}) + (p_{up} + p_{down} + p_{wind}))$$

where *n-1* is the adjacent upstream (coastside) pixel, t_{up} and t_{down} are the terrain penalties for uphill and downhill flow paths, respectively; p_{wind} is the coastal path length penalty for each pixel traveled, scaled by a wind direction frequency value; and p_{up} and p_{down} are additional path length penalties for uphill and downhill flow paths, respectively.

Parameter settings were based on results from other coastal simulations and comparisons of model output with station data in Puerto Rico coastal areas (Table I). Terrain parameters reflect the assumption that as the terrain barrier increases in size, the potential for loss of momentum leads to an increased likelihood that the air will follow a path around the barrier, if possible. Pathlength penalties reflect the effects of slope on the modification of coastal air parcels (Table I). Coastal intrusions often transport moist air inland; when this air follows an uphill path, the relative humidity is likely to increase as the air cools adiabatically, creating a milder, more "coastal" environment, possibly characterized by clouds and mist; hence a decrease in the CI score. However, when this airflow encounters downslope conditions, adiabatic warming may produce the opposite effect, and accelerate the warming and drying process.

Table I. Parameter values used in the application of the PRISM coastal advection and trajectory preprocessor models to Puerto Rico. h is the terrain height difference in meters between a pixel and its upstream neighbor; a positive h denotes upslope conditions. See text for details and definitions of parameters.

Model	t_{up}	t_{down}	p_{up}	P_{down}	P_{wind}	p
Coastal Advection (Temperature)	$0.2h$	0.0	$-0.05h$	$0.5h$	See text	NA
Trajectory (Precipitation)	$0.1h$	$0.3h$	NA	NA	NA	0.5/pixel

The wind-aided path length penalty, p_{wind}, is smallest for the most frequent wind directions and largest for the least frequent directions. An analysis of general flow patterns in the vicinity of Puerto Rico, and a comparison of advection model results with station data, suggested that the flow was predominantly out of the east. Since adjacent pixel directions are modeled on an eight-point compass, the easterly flow direction was given a p_{wind} value of 1. A NE flow path, the next most frequent direction, was given a p_{wind} value of 5, with NW and SE directions assigned 10 and S, SW, and W assigned 20.

Once the initial paths were established, the advection model used an iterative procedure to find an optimized route between each land pixel and the coastline, sometimes resulting in preferred routes that sacrificed short path lengths for less terrain complexity. At the end of the simulation, each land pixel had been assigned the lowest CI score possible. The CI values were $\log_{10}$-transformed to help normalize gradients over the region. The resulting grid served as the PRISM coastal proximity grid (Figure 2a). In the PRISM simulation, stations with CI scores similar to that of the target pixel were given more weight in the moving-window climate-elevation regression function than those that had very different CI scores.

2.3.3. Coastal Proximity Guidance – Trajectory Model for Moisture Availability

Preliminary analysis of spatial patterns in the precipitation data showed significant windward-leeward gradients (i.e., rain shadows) caused by airflow over Puerto Rico's complex terrain. A simple trajectory model designed for PRISM was used to assess relative moisture availability to guide precipitation mapping. This method of determining terrain-based precipitation regimes gave more suitable results than topographic facet weighting (Daly *et al*., 2002), because of the complexity of the terrain and the relatively sparse station data set. The trajectory model is similar to the coastal advection model, in that it accounts for changes in moisture content due to path length and terrain effects. It differs in that the air parcel trajectories are straight-line and invariant throughout the simulation, as might be the case during large-scale circulations that produce significant precipitation. The premise here is that the mean potential for precipitation experienced at a site is the result of: (1) loss of moisture through rainout, which accumulates as the path length over land increases (hereafter called the path length penalty); and (2) enhancement and suppression of precipitation caused by adiabatic cooling and warming during flow over terrain obstacles (hereafter called the terrain penalty).

To begin the simulation, ocean pixels along the coastline were assigned a "Precipitation Index" (PI) score of 0. The original unfiltered, rather than the 2.5-minute filtered, DEM was used to describe the terrain. However, the terrain was effectively smoothed to this wavelength through the model's constant lateral mixing of air out to a distance of 1.25 minutes (~2.5 km) on either side of the trajectory.

The PI score at pixel n was calculated as follows:

(4) $$PI_n = PI_{n-1} + t_{up} + t_{down} + p$$

where *n-1* is the adjacent upstream pixel, t_{up} and t_{down} are the terrain penalties for uphill and downhill flow paths, respectively; and *p* is the path length penalty for each pixel traveled.

Parameter settings were based on results from Hawaiian Island simulations and comparisons of model output with Puerto Rico precipitation data (Table 1). In general, upslope terrain causes vertical uplift, adiabatic cooling, and increased condensation and precipitation. Downslope terrain dampens vertical velocity and dries the air parcel through adiabatic warming. The trajectory model allows for a 10-km upwind coastal precipitation enhancement region to account for viscosity in the airflow. As the air parcel approaches land, the model searches up to 10 km downstream for upslope terrain features that could cause early lifting of the air stream, enhancing precipitation over the coastal lowlands. Based on predominant wind directions found for the coastal advection simulation, the trajectory model was run for two trajectory directions, NNE and NE, and the results averaged to produce the final PI grids. As will be seen in the Results section, flow patterns vary markedly from month to month, resulting in large-scale precipitation patterns that also vary markedly. However, the PI index is designed to provide a guide to PRISM only in identifying similar regimes within a localized area (i.e., within a 20-km radius) that is within the search region for stations around a given pixel; these localized areas of similarity are relatively less variable over time.

A comparison of the PI grid with station precipitation data revealed that there was an observed decrease in precipitation near the coastlines that was not accounted for in the PI grids. This was thought to result from suppression of convective activity in coastal areas, which experience reduced surface heating. This effect was added by scaling and combining the PI grid with the CI grid produced by the coastal advection model. This combined PI-CI grid (Figure 2b), was used as the "coastal proximity" input to the PRISM precipitation simulations. The PI-CI grid no longer matched patterns of precipitation in the way that the PI grid did, but was deemed more useful as a guide in locally weighting nearby stations in a grid cell's regression function. Stations with PI-CI scores similar to that of the target pixel were given more weight in the moving-window precipitation-elevation regression function than those that had very different PI-CI scores.
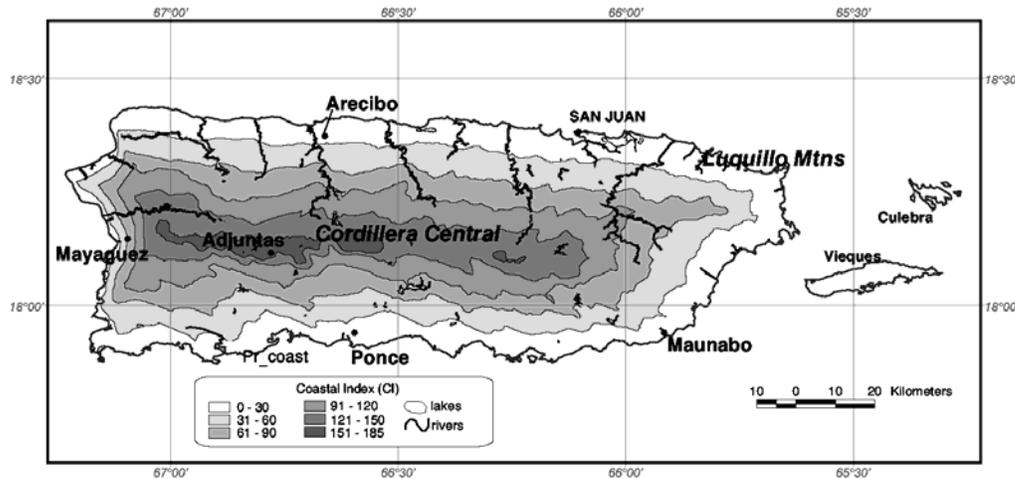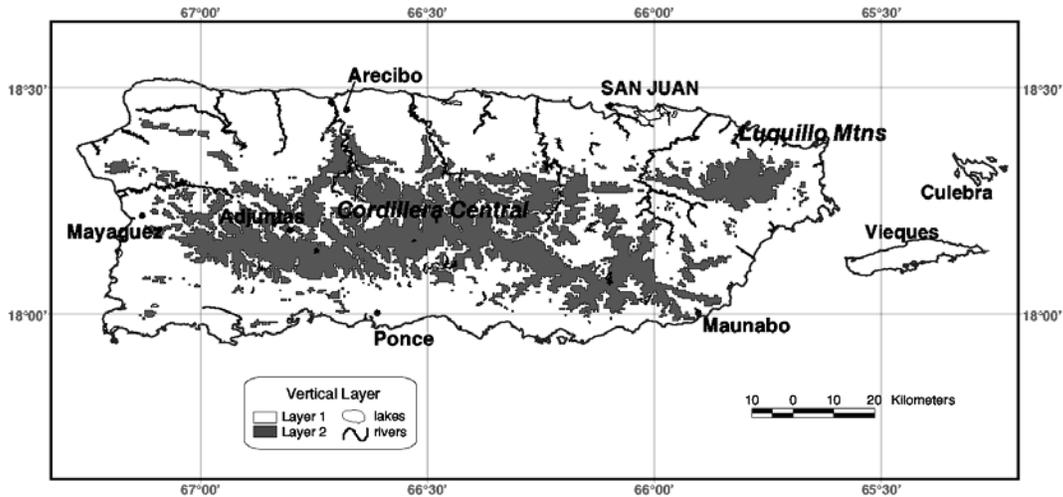

(a)
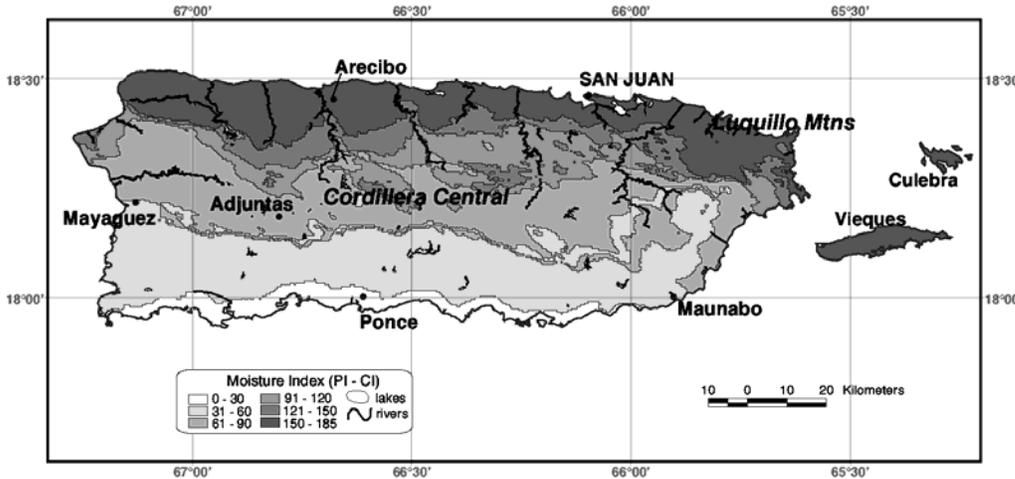
(b)

Figure 2. Supplementary input grids used for interpolation guidance: (a) coastal index for temperature mapping; (b) combined precipitation-coastal index for precipitation mapping

(c)

Figure 2. (Continued) Supplementary input grids used for interpolation guidance: (c) atmospheric layer for minimum temperature mapping.

2.3.4. Vertical Layer Guidance

Despite the oceanic nature of the temperature regimes on Puerto Rico, elevated inland valleys sheltered from coastal influences by terrain barriers (e.g., Adjuntas) exhibited relatively low minimum temperatures despite their low elevation, especially during winter. This pattern, common to interior valleys at mid-latitudes (Daly *et al.*, 2002), is caused by the pooling of cool air draining from surrounding mountains at night. Minimum temperatures in these valleys are typically as low or lower than adjacent hill slopes and ridge tops at higher elevations. These conditions dissipate with the advent of surface heating during the day. Observations in Puerto Rico indicated that the height of the inverted or isothermal layer was typically about 150 m above the valley floors. To simulate such conditions for minimum temperature mapping, climate station data entering the PRISM regressions were divided into two vertical layers. A grid depicting the height of layer 1, the boundary layer, was calculated as 150 m above the lowest grid cell within a 5 km radius (Figure 2c). This division is only a potential one; at each pixel, PRISM tests the regression functions in layers 1 and 2 to assess their differences and similarities, and sets the layer-weighting exponent accordingly. If very different, the weighting exponent is high and stations in one layer are downweighted when used in a regression function for the other layer. If similar, stations from both layers are given similar weights (Daly *et al.*, 2002).

2.3.5. Effective Terrain Weight Guidance

A grid to weight regressions for effective terrain height was developed to quantify the relative effectiveness of terrain features on Puerto Rico in producing vertical gradients in precipitation. Most of Puerto Rico was designated as having terrain that would produce significant three-dimensional precipitation gradients, with the exception of the coastal plains, where terrain features are more subdued (Figure 1). More

information on effective terrain height calculation and use in PRISM is available from Daly (2002).

2.3.6. PRISM Simulations

PRISM simulations were performed on a monthly basis for mean daily maximum and minimum temperature, and total precipitation, using station data summarized for the period 1963-1995. An annual total precipitation grid was calculated by summing the monthly grids. At least 20 stations were used in each of the 47,327 (1 per grid cell), moving-window regression functions per month per climate variable.

National Weather Service Cooperative station locations were given to only the nearest 60 arc-seconds (~2 km), which is a low spatial precision in comparison with the 15 arc- second (~450m) grid cell size of our simulation grid. To minimize the effects of imprecise station locations on the simulations, a PRISM option was exercised that initiated a search within a 60-second window for the best match between the 15-second DEM elevation and the station elevation given in the metadata. The search started at the coordinates given in the metadata, and spiraled outward at small increments until a match was found. The station was then reassigned the location where this match occurred. If no match was found within the specified window, the station location was reassigned to the location with the best elevation match.

Two alternative PRISM parameterizations were compared for each climate variable. For temperature, the standard PRISM parameterization (hereafter abbreviated as PRISM), was compared to one in which the slope was fixed at –6.5°C/km elevation. This is the approximate rate of cooling of a standard atmosphere between 0 and 1000m elevation, using hypsometric relationships (Ahrens, 2003). For the hypsometric parameterization (hereafter abbreviated as HYPS), coastal proximity, vertical layer, and elevation weighting were disabled, and distance and cluster weighting were kept active. The goal of HYPS was to approximate a simpler, commonly used interpolation method, in which: (1) each station's temperature is adjusted to sea level using a constant –6.5°C/km slope; (2) the adjusted "sea-level" temperatures are interpolated with an inverse-distance weighting function; and (3) the interpolated grid is adjusted to the DEM elevations using the same –6.5°C/km slope to produce the final temperature grid.

For precipitation, the standard PRISM parameterization was compared to an inverse-distance weighting (hereafter abbreviated as IDW) interpolation, which is the most commonly used method to map precipitation. To approximate this method, the PRISM input DEM was replaced with one with zero values (sea level) only; coastal proximity, vertical layer, and elevation weighting were disabled; and distance and cluster weighting were kept active.

2.3.7. Performance Evaluation

The performance of the alternative interpolation approaches was evaluated using jackknife cross-validation with replacement. Jackknife cross-validation involves omitting a data point, estimating temperature or precipitation at that point and comparing the predicted to the observed values, replacing that data point, and proceeding to the next data point. This procedure was repeated until all station data points had been predicted in their absence. Coefficient of determination (r^2), slope (b_1) y-intercept (b_0), bias, mean absolute error (*MAE*), root mean square error (*RMSE*), proportion of systematic error

(*PSE*), coefficient of efficiency (*E*), and index of agreement (*d*) were calculated for each method. r^2 describes the proportion of the total variance in the observed data that can be explained by the model. b_1 and b_0 describe the linear relationship between predictions and observations. Bias is the mean of the signed difference between prediction P_i and observation O_i. *MAE* is the mean of the unsigned differences between P_i and O_i. *RMSE* is the square root of the mean of the squared residuals. *PSE* is the ratio of the systematic, or model, error to the total error, and is calculated as MSE_s / MSE, where *MSE* is the total mean square error, and MSE_s is the systematic error, written as

$$(5) \qquad MSE_s = \frac{\sum_{i=1}^{N}\left|\hat{P}_i - O_i\right|^2}{N-1}$$

where $\hat{P}_i$ is the prediction of O_i using the ordinary least squares regression function described by b_1 and b_0. *E*, the coefficient of efficiency, is the ratio of the mean square error to the variance in the observed data, subtracted from unity (Legates and McCabe, 1999). It has a range of minus infinity to 1.0, with higher values indicating better agreement. *d*, the index of agreement, is given as

$$(6) \qquad d = 1.0 - \left[\frac{\sum_{i=1}^{N}(O_i - P_i)^2}{\sum_{i=1}^{N}(\left|P_i - \overline{O}\right| + \left|O_i - \overline{O}\right|)^2}\right]$$

where $\overline{O}$ is the mean observed value. *d* ranges between 0 – 1.0 with higher values indicating better agreement. Reviews of these statistics for model evaluation can be found in Willmott et al (1985) and Legates and McCabe (1999).

3. RESULTS AND DISCUSSION

3.1. Temperature

Spatial patterns in temperature were linked primarily to elevation, topographic position, and proximity to the ocean. Minimum and maximum temperature generally decreased with elevation in all months (Table II, Figures 3-4). January minimum temperatures were warmest along the coastal strip, due to the moderating influence of the ocean (Figure 3). Maximum temperatures did not show an obvious coastal pattern, but did tend to be the warmest in areas receiving relatively little precipitation on an annual basis, where cloudiness was presumably lower, solar radiation greater, and a greater proportion of the solar radiation used for sensible heat generation, rather than moisture evaporation (Figure 4). Elevated inland valleys sheltered from coastal influences by terrain barriers exhibited relatively low minimum temperatures, especially during winter. In the Adjuntas area, minimum temperatures were less than 13ºC during January through March (Figure 3), due to cold air drainage into this basin. A trend towards smaller

elevational gradients of minimum temperature in the interior of Puerto Rico was reflected in the region-wide mean temperature-elevation slopes for minimum temperature (Table II). The mean layer 1 (boundary layer) slope reached a minimum magnitude of -2.9ºC/km from December through February and a maximum magnitude of –4.2ºC/km in May. Layer 2 (free atmosphere) slopes were a more consistent –4.0 to –4.9ºC/km. In contrast, maximum temperature slopes maintained a constant –7.1 to -7.3ºC/km throughout the year.

Comparison of the PRISM and HYPS results showed that both methods produced generally similar patterns of temperature (Figures 3-4). The greatest differences occurred in the January minimum temperature patterns. The HYPS map (Figure 3b) exhibited a larger area of low minimum temperature in the interior than the PRISM map (Figure 3a). This was due to the use in HYPS of a constant temperature/elevation slope of –6.5C/km, rather than the actual slope, which was much smaller in the coolest interior valleys. A lack of coastal proximity weighting in HYPS caused cooler minimum temperatures to edge into coastal zones where coastal observations were lacking, whereas PRISM better maintained the integrity of the warm coastal zone by preferentially using other coastal stations, with warmer temperatures, in its predictions. Performance statistics for January minimum temperature show consistently the predictive skill of PRISM to be greater than that of HYPS (Table 3). HYPS had relatively poor predictive capability at lower end of the temperature range (Figure 5), due to a lack of layer weighting and the use of the constant temperature/elevation slope of –6.5C/km. Both methods predicted the warmest minimum temperatures reasonably well, with HYPS showing slightly less scatter than PRISM.

Both PRISM and HYPS performed well for July maximum temperature (Figures 4 and 6, Table 3). Performance statistics were similar, except for b_1, b_0 and PSE. The proportion of the mean square error that was systematic was 12 percent for PRISM , but 34 percent for HYPS. This is illustrated by the scatterplot (Figure 6), which shows that while the overall scatter was low, there was a systematic tendency for HYPS to over-predict temperatures at the lower end of the range (hence a high b_0 and low b_1). Over-prediction of temperatures at high elevations is consistent with the use of the fixed –6.5C/km slope, which is a somewhat lesser decrease in temperature with elevation than the actual slope, which averages –7.5C/km (Table II).

The spatial distributions of temperature cross-validation errors for PRISM are shown in Figure 7. Relatively high errors in January minimum temperature occurred in the San Juan area, due to a tight and complex gradient in temperature around the city and to the south. There appeared to be local effects, possibly related to urban patterns, influencing some of these sites. Another region of higher error was in the Adjuntas area, where large gradients in temperature were caused by local cold air drainage patterns. Here, each station played an important role in defining the temperature patterns, and surrounding stations did not provide sufficient information to predict a station well in its absence. Cross-validation errors were generally small for July maximum temperature. A relatively large error did occur at Pico Del Este, an isolated high-elevation station in the Luquillo Mountains. The nearest high-elevation station to Pico Del Este was located in the southeastern portion of the Cordillera Central, in a warmer and drier regime. Therefore, in its absence, the July maximum temperature at relatively cloudy and cool

Pico Del Este was over-predicted. This points up the importance of this station in defining the temperature regime in the Luquillo Mountains.

Averaging the PRISM minimum and maximum temperature grids for each month, then averaging across all months, yielded a mean annual temperature map (Figure 8). Spatial patterns are similar to those of the monthly maps, with the lowest temperatures occurring at high elevations in the interior, and highest temperatures restricted to the coastal lowlands. The mean annual temperature ranges from over 26ºC along the northeast and south coasts, to less than 20ºC at the highest elevations of the Cordillera Central and Luquillo Mountains. This map was compared to an official map published in 1969 by what was once the U.S. Department of Commerce's Environmental Sciences Service Agency (ESSA, 1969a), and reproduced in NOAA (1974). This map was drawn by hand, with guidance provided by station data representing the 1931-60 averaging period. It is highly smooth and generalized. The two main features were a large, narrow, east-west oriented temperature minimum roughly corresponding to the Cordillera Central; and a small, oval-shaped minimum over the Luquillo Mountains. The lowest temperature indicated at these minima was 20ºC. Smaller-scale ridges and mountaintops were ignored. Warmer isothermal contours generally paralleled the coastline. Temperatures reached a maximum of about 26ºC along the southern and northeastern coastlines. The range of temperatures on the ESSA map was very similar to that of the PRISM map.

Table II. Maxima, means, minima, and altitudinal slopes for temperature and precipitation calculated by PRISM (full parameterization). Values are for all grid cells in the Puerto Rico-Vieques-Culebra modeling domain (N=47327). Slopes are the means of the moving-window, climate-elevation regression slopes for all grid cells in the modeling domain; n>=20 stations for each regression

|	Jan	Feb	Mar	Apr	May	Jun	Jul	Aug	Sep	Oct	Nov	Dec	Ann
Element													
Maximum Temperature													
Max (°C)	31.2	31.5	31.7	32.6	32.7	33.4	33.6	33.7	33.4	33.2	32.2	31.2	32.4
Mean (°C)	28.1	28.4	28.8	29.4	29.9	30.6	30.7	31.0	30.6	30.6	29.6	28.4	29.7
Min (°C)	20.1	20.2	20.7	21.1	21.7	22.7	23.2	23.3	23.1	22.6	21.5	20.3	21.7
Slope (°C/km)	-7.3	-7.2	-7.1	-7.3	-7.3	-7.5	-7.4	-7.3	-7.1	-7.2	-7.3	-7.3	-7.3
Minimum Temperature													
Max (°C)	21.7	21.4	21.8	22.6	23.6	24.4	24.8	24.7	24.6	24.1	23.3	22.2	23.2
Mean (°C)	17.5	17.4	17.8	18.5	19.9	20.8	20.9	20.9	20.8	20.4	19.5	18.3	19.4
Min (°C)	12.7	12.4	12.5	13.5	14.7	15.6	15.7	16.1	15.8	15.5	14.6	13.5	14.6
Slope (°C/km)													
Layer 1	-2.9	-2.9	-3.1	-3.3	-4.2	-3.9	-3.5	-3.7	-3.3	-3.7	-3.1	-2.9	-3.4
Layer 2	-4.5	-4.6	-4.8	-4.5	-5.0	-5.0	-5.0	-4.8	-4.6	-4.6	-5.1	-4.7	-4.8
Precipitation													
Max (mm)	341	320	278	314	506	386	399	433	420	468	512	450	4598
Mean (mm)	76	68	79	120	196	130	137	181	201	219	172	108	1687
Min (mm)	21	15	18	26	69	35	34	81	67	108	77	24	701
Slope (mm/km)	103	89	113	180	305	187	187	233	299	325	192	132	2345
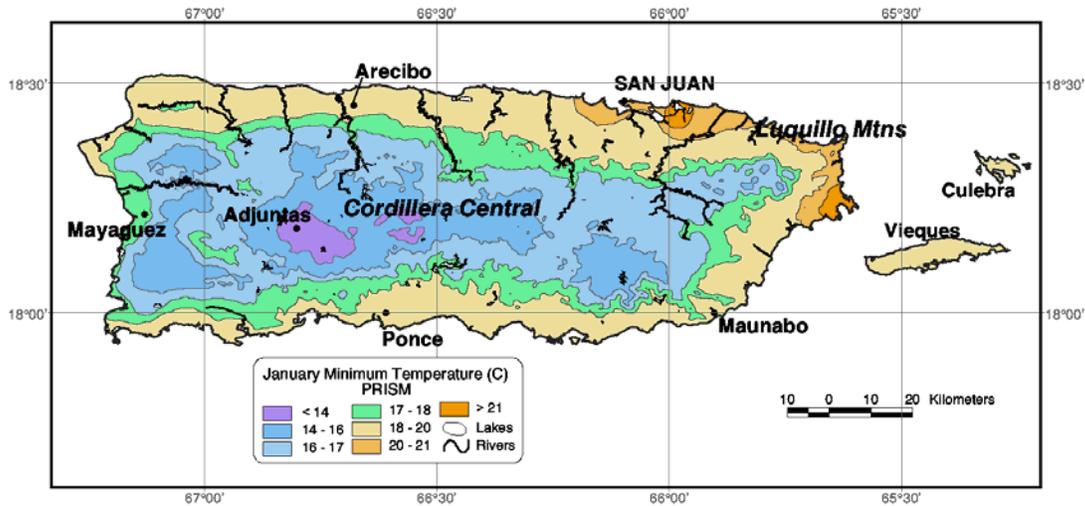
(a)
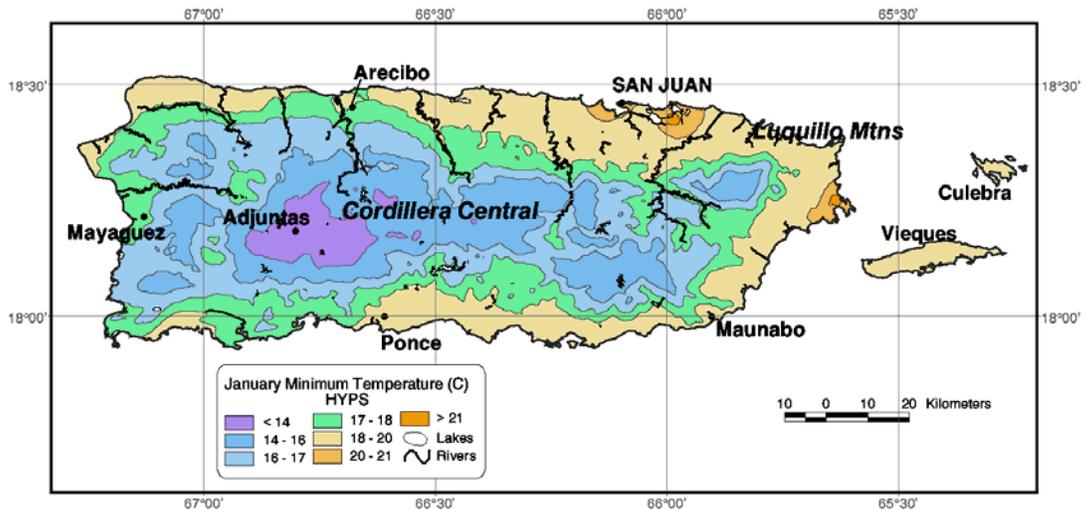
(b)

Figure 3: Mean 1963-95 January minimum temperature for Puerto Rico, Vieques, and Culebra: (a) PRISM; (b) HYPS

The largest difference between the two was the level of detail: the PRISM map, based on a 450-m DEM, possessed much more spatial detail than the ESSA map.
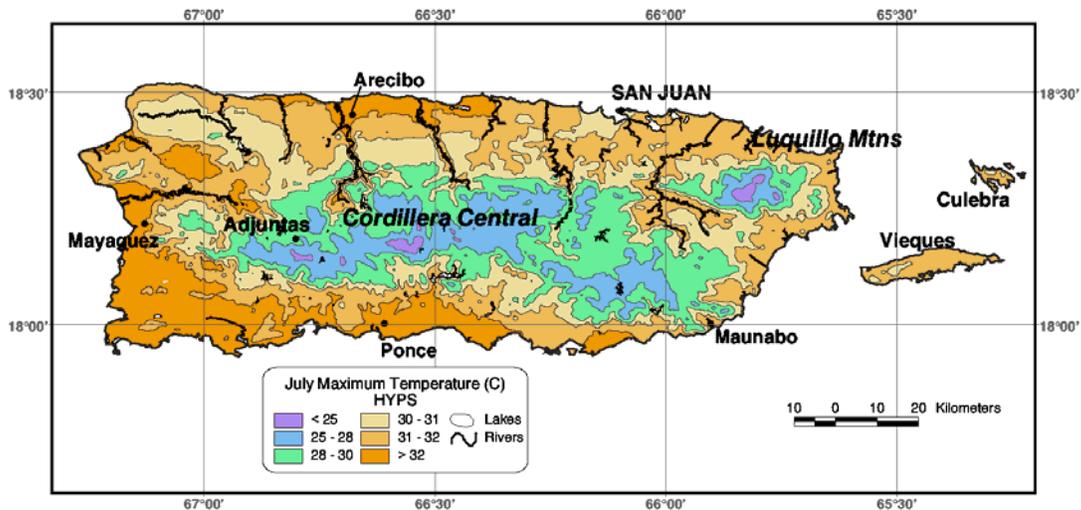
3.2. Precipitation

Mean monthly precipitation varied significantly throughout the year (Figure 9, Table II, reflecting seasonally differing moisture trajectories. The winter months were generally driest. In January, precipitation was greater than 70 mm only over the northern and eastern parts of Puerto Rico. However, the Luquillo Mountains received over 300 mm. April precipitation was generally greater than that of January. The greatest increases over January occurred on the lower, northern slopes of the Cordillera Central, but the south

coast remained relatively dry. July exhibited a split precipitation pattern, with maxima occurring on both the western and eastern ends of the island. October was the wettest
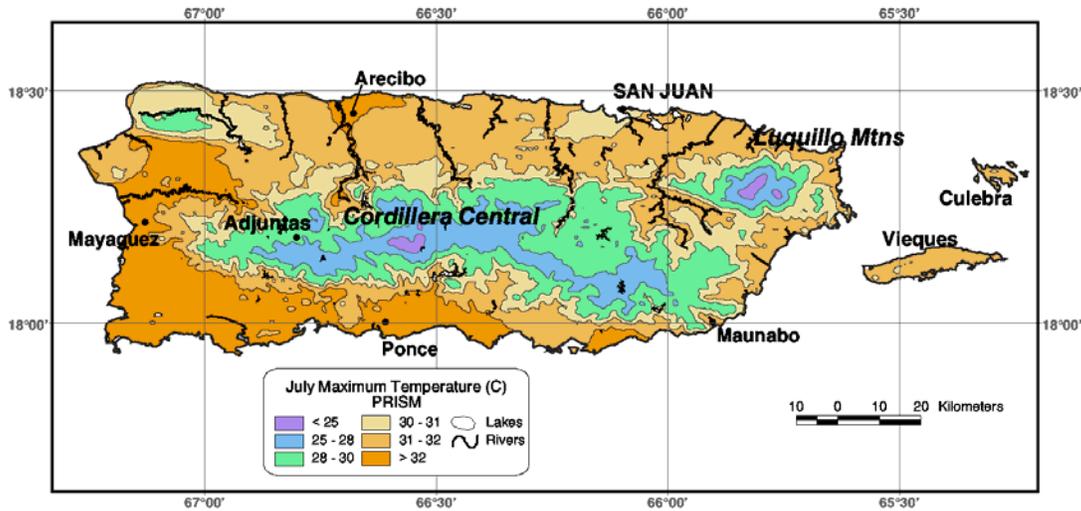
(a)

(b)

Figure 4: Mean 1963-95 July maximum temperature for Puerto Rico, Vieques, and Culebra: (a) PRISM; (b) HYPS

month overall, mainly because precipitation was abundant over most of the island. Moisture reached the island from many directions, markedly reducing the north-south rain shadow effect of the Cordillera Central. Orographic effects dominated the spatial patterns, with the largest precipitation totals occurring on the highest peaks of the Cordillera Central and the Luquillo Mountains.

Elevational gradients of precipitation followed the mean values closely, being lowest during the drier winter months and greatest during May, late summer and early

fall (Table II). In general, precipitation increased at a rate of approximately 140% of the average amount per km elevation. These slopes were somewhat higher than those in the western US, where slopes were observed to range from 80 to 112% per km (Daly *et al.*, 1994). However, limited data from PRISM modeling studies on tropical Pacific Islands indicated that slopes of 100-150% per km were not uncommon.

Table III. Performance statistics for standard and alternative parameterizations of PRISM as applied to Puerto Rico January minimum and July maximum temperature, and precipitation. N=50 for minimum temperature, 47 for maximum temperature, and 108 for precipitation. See text for definitions of model parameterizations and performance statistics.

	r^2	b_0	b_1	Bias	MAE	RMSE	PSE	E	d
January Minimum Temperature		(°C)		(°C)	(°C)	(°C)	(%)		
PRISM	0.72	3.83	0.78	0.02	0.97	1.24	18	0.72	0.92
HYPS	0.55	5.05	0.69	-0.03	1.26	1.66	21	0.50	0.85
July Maximum Temperature									
PRISM	0.92	2.97	0.90	0.03	0.53	0.68	12	0.92	0.98
HYPS	0.91	5.56	0.82	0.01	0.56	0.76	34	0.90	0.93
Annual Precipitation		(mm)		(%)	(%)	(%)	(%)		
PRISM	0.88	240.67	0.84	0.5	10.8	13.6	17	0.85	0.96
IDW	0.70	753.39	0.57	7.1	16.2	21.9	57	0.68	0.88

On an annual basis, cumulative spatial precipitation patterns were associated most strongly with elevation, upslope exposure to predominant moisture-bearing winds, and proximity to the ocean (Figure 10a). The Cordillera Central was a major barrier to the generally north-to-northeasterly moisture-bearing flow, enhancing precipitation on its northern (windward) slopes and producing a rain shadow on its southern (leeward) slopes. Four major centers of maximum annual precipitation were evident (Figure 10): the Luquillo Mountains in the northeast, the hills of the southeast, the higher peaks of the Cordillera Central, and the hills of the northwest. The Luquillo Mountains, rising steeply from the northeastern coastline and exposed to the ocean on three sides, is the first topographic barrier encountered by moisture-bearing winds moving onshore. The result is strong and frequent orographic uplift and easily the highest precipitation totals on Puerto Rico. In contrast, the driest conditions on the island were located along the southern coastline. Here, terrain features are minimal, and mountains block moisture from all directions but the south. Smaller, less pronounced precipitation minima occurred on the northwest coast, an area that has abundant moisture but is not affected strongly by orographic enhancement, and in a valley in the eastern interior that is somewhat sheltered from moist, oceanic intrusions by hills on all sides.

Comparison of mean annual precipitation maps produced by the PRISM and IDW parameterizations showed similar broad-scale patterns, but significantly different details (Figure 10). Precipitation patterns produced by the IDW method were dictated by the values and locations of the data points, rather than the underlying topography or moisture

regime. This produced a series of "bulls eyes" across the IDW map, with little recognizable structure (Figure 10b). In contrast, the PRISM map showed no bulls eyes, but rather physically consistent patterns that followed elevation and moisture availability zones (Figure 10a). Since there is no elevation extrapolation of precipitation in the IDW parameterization, precipitation maxima were lower and minima higher in the IDW map than in the PRISM map. Dry interior valleys were largely missing from the IDW map, as
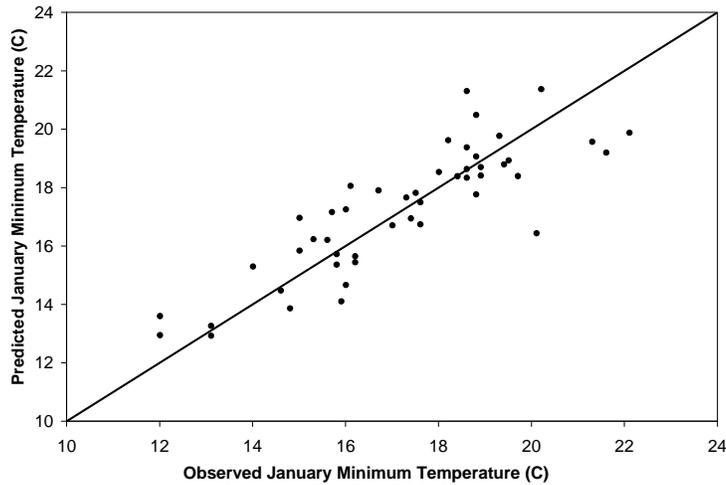

(a)
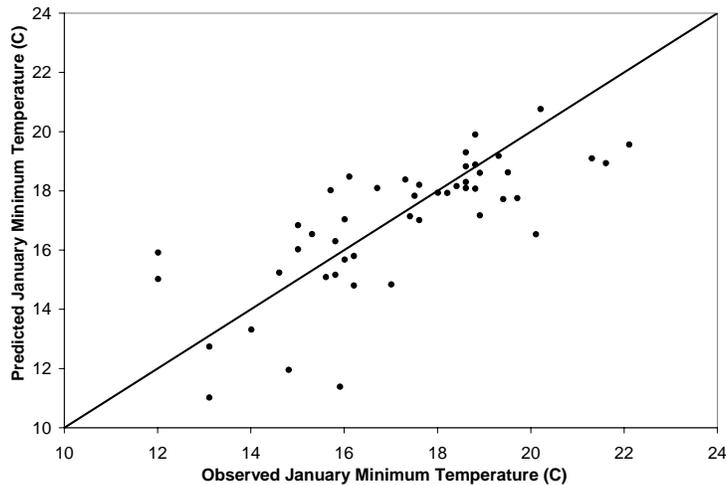
(b)

Figure 5. Scatterplots of predicted versus observed mean 1963-95 January minimum temperature for Puerto Rico, Vieques, and Culebra: (a) PRISM; and (b) HYPS.

were topographically enhanced wet zones south of San Juan and in the western mountains. All performance statistics and scatterplots of predictions and observations show that the IDW performed poorly compared to PRISM (Table III, Figure 11). Bias statistics indicate that, on average, IDW over-predicted by over 7 percent (Table III), compared to 0.5 percent for PRISM. This is confirmed by the scatterplots in Figure 11, showing that most of the IDW predictions are above the 1:1 line, especially at low

precipitation amounts, while the PRISM predictions are more equally distributed above and below the 1:1 line. The tendency for IDW to over-predict is systematic, as illustrated by PSE, which is 57 percent for IDW, compared to 17 percent for PRISM. IDW's over-predictions occurred most commonly along the coast, where dry coastal sites, when omitted in the cross-validation exercise, were over-predicted using wetter mountain sites in close proximity to the coastline. In contrast, PRISM's moisture availability guidance downweights these wetter stations in favor of more distant, but climatically similar, coastal sites, and uses an elevation regression function to reduce the higher-elevation precipitation values to coastal levels.
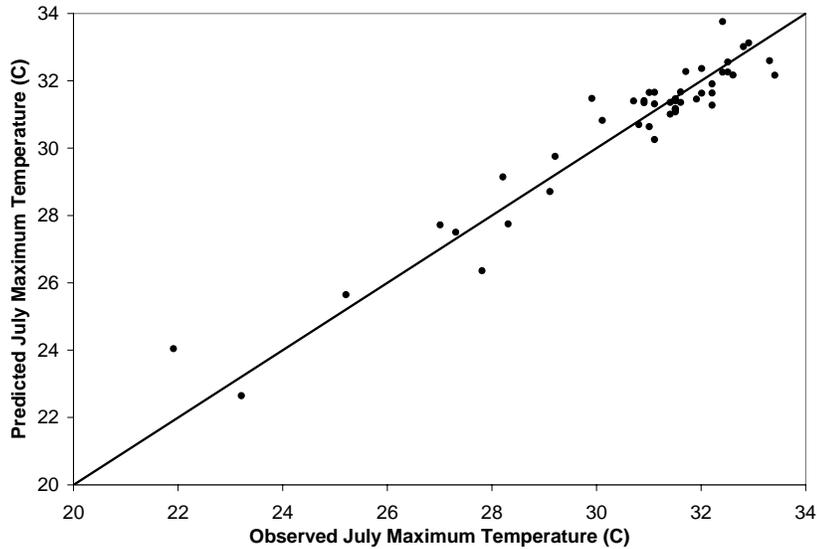
(a)
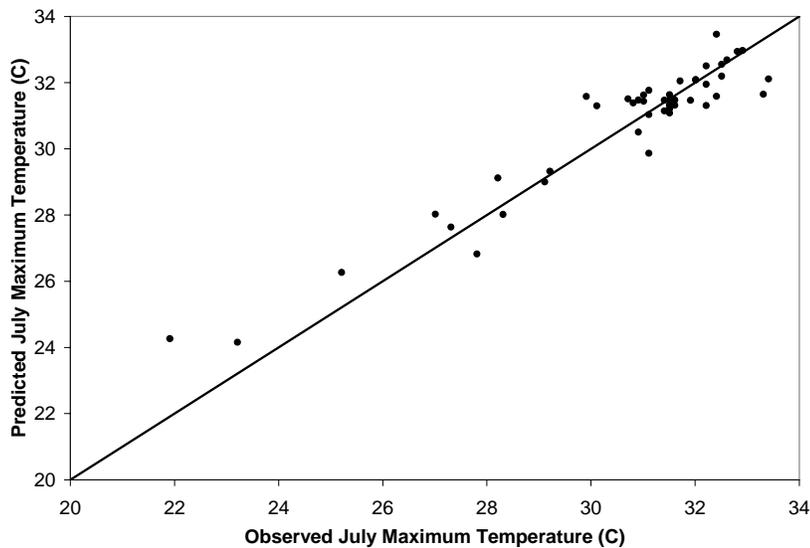
(b)

Figure 6: Scatterplots of predicted versus observed mean 1963-95 July maximum temperature for Puerto Rico, Vieques, and Culebra: (a) PRISM; and (b) HYPS.

The spatial distributions of annual precipitation cross-validation errors for PRISM are shown in Figure 12. There is little regional pattern to the errors, but the highest errors tend to occur where spatial precipitation gradients are greatest and there is the most the most station-to-station variability in precipitation.

The PRISM mean annual precipitation map in Figure 10 was compared to an official map published in 1969 by what was once the U.S. Department of Commerce's Environmental Sciences Service Agency (ESSA, 1969b), and reproduced in NOAA (1974). As with temperature, this map was drawn by hand, with guidance provided by station data representing the 1931-60 averaging period. The ESSA map depicted the same four main precipitation maxima and the south-coast minimum that existed on the PRISM map, but the patterns were much broader and more generalized. Amounts were largely similar, as well. The three 2500-mm maxima in the northwest, southeast, and the Cordillera Central shown on the PRISM map were also depicted as 2500-mm on the ESSA map. The Luquillo Mountains maximum was estimated at 4500-5000 mm, compared to 4500 mm on the PRISM map. This slight difference may be explained by additional data used in the current map that were not available previously. The PRISM maximum was essentially the same as the 4500-mm maximum estimated for the crests of the Luquillo Mountains by Garcia-Martino, et al. (1996a). The south-coast minimum was less than 850 mm on both the PRISM and ESSA maps. Closely matching amounts indicate that annual average precipitation during the 1931-60 period was similar to that of the 1963-1995 period.
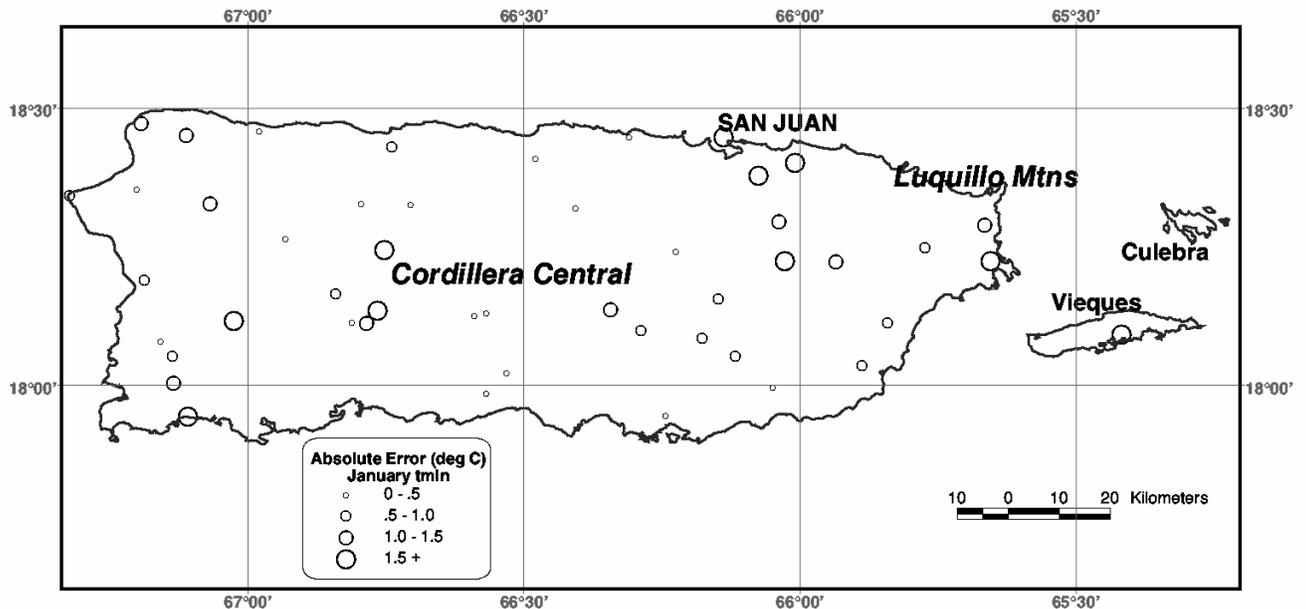
(a)

Figure 7. Cross-validation errors for mean 1963-95 (a) minimum January temperature for Puerto Rico, Vieques, and Culebra, PRISM parameterization
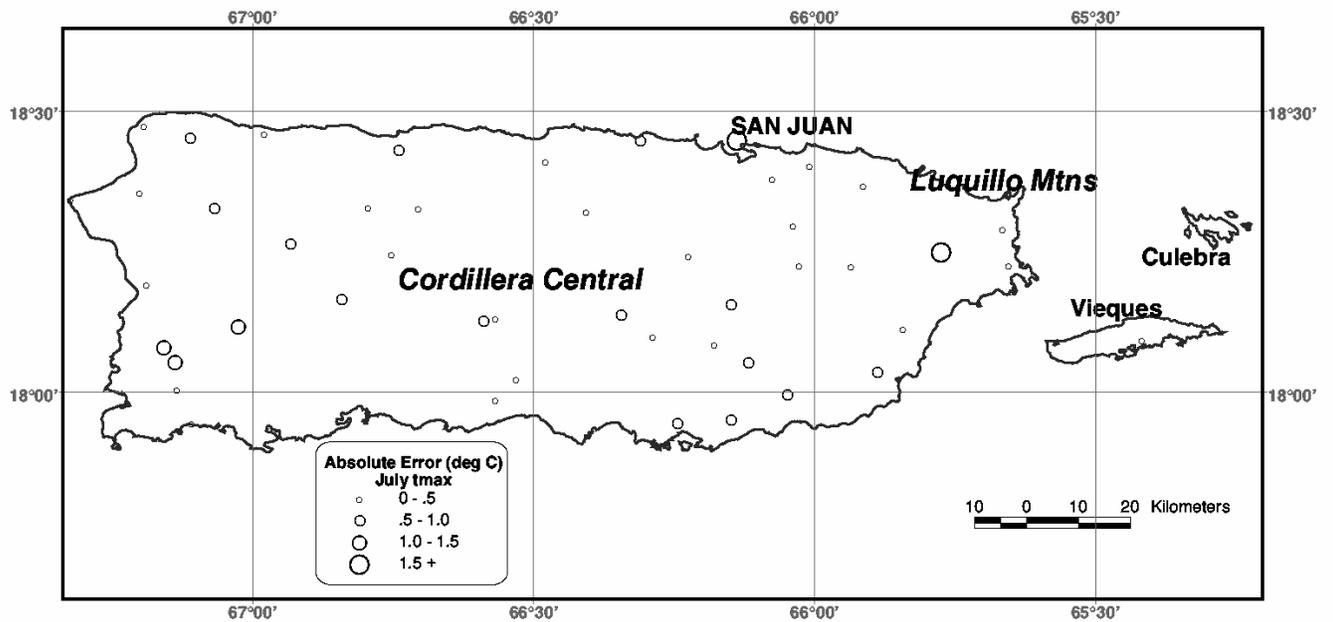
(b)

Figure 7. (Continued) Cross-validation errors for mean 1963-95 (b) July maximum temperature for Puerto Rico, Vieques, and Culebra, PRISM parameterization
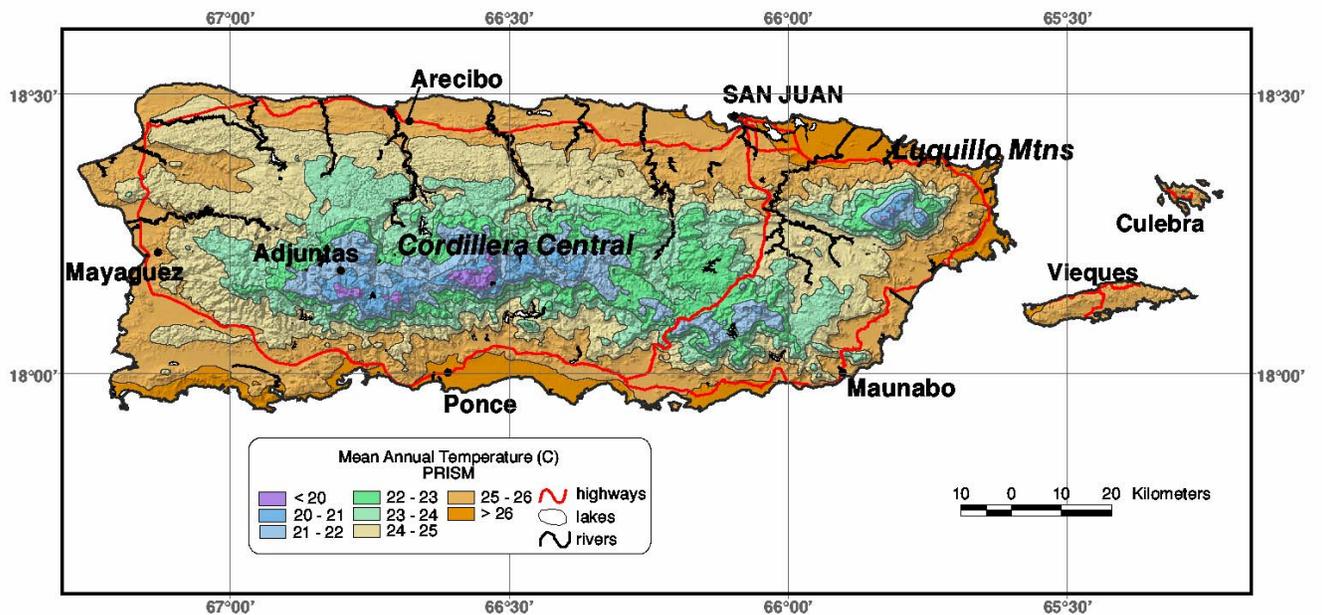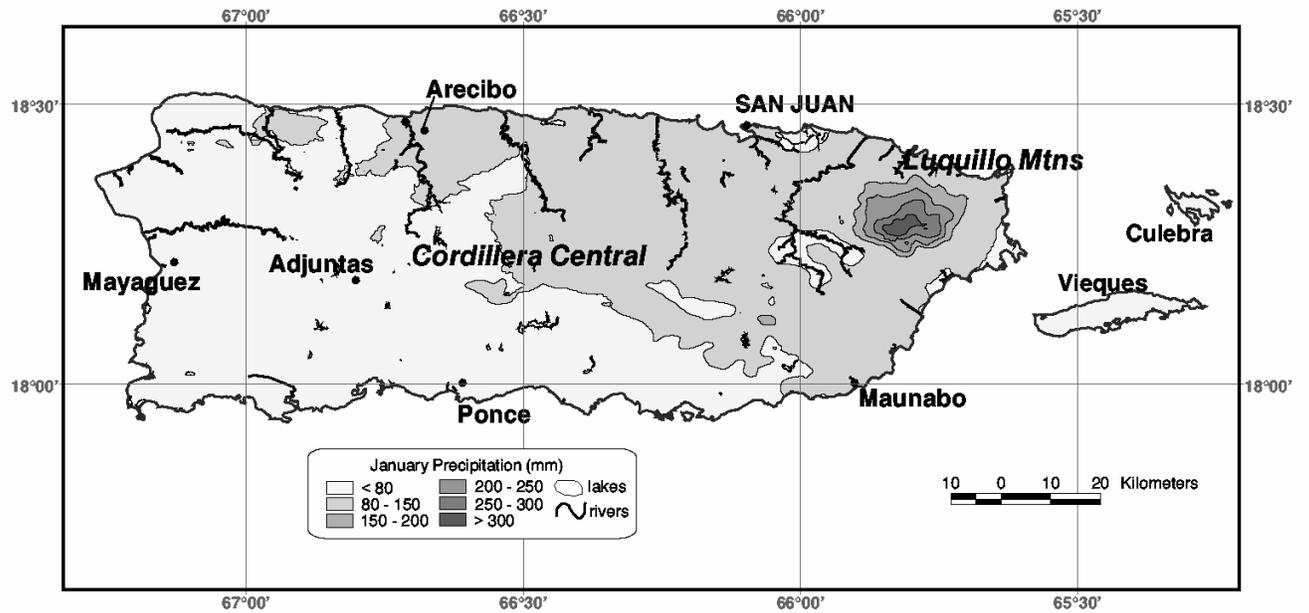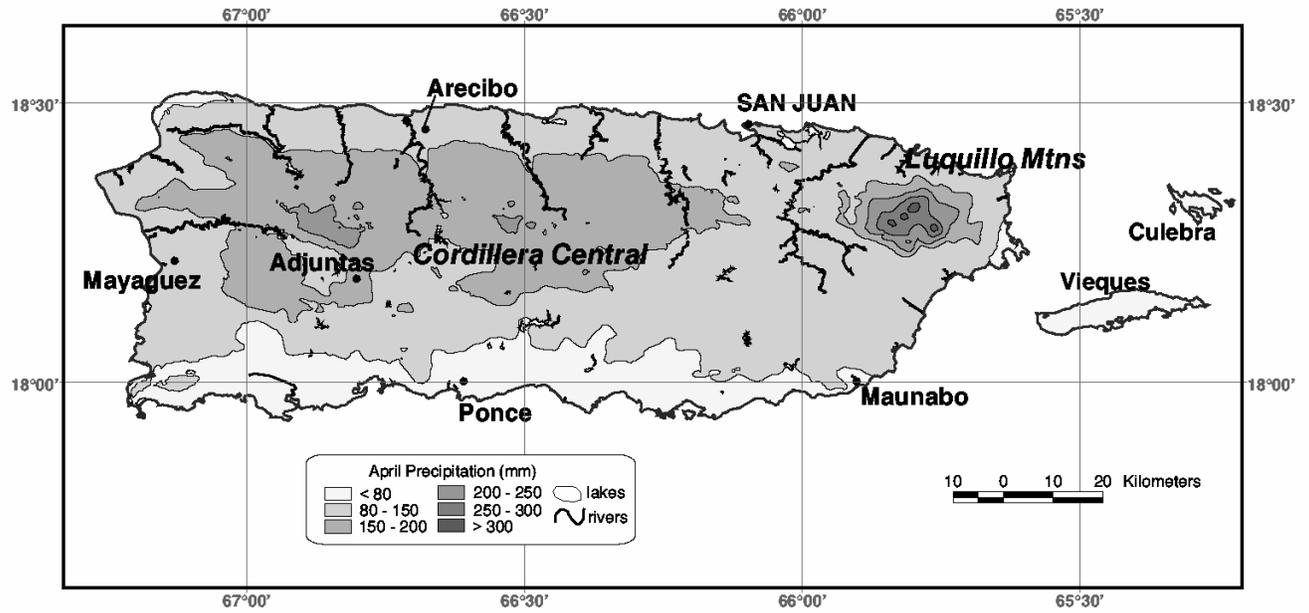

Figure 8. Mean 1963-95 annual temperature for Puerto Rico, Vieques, and Culebra; PRISM parameterization
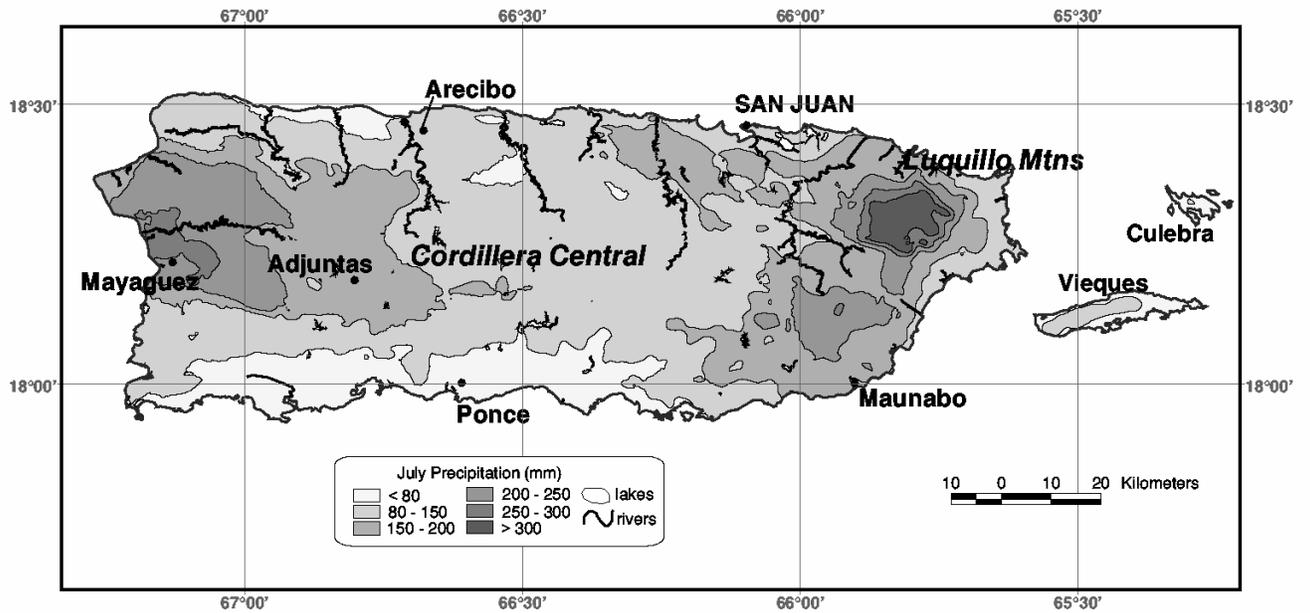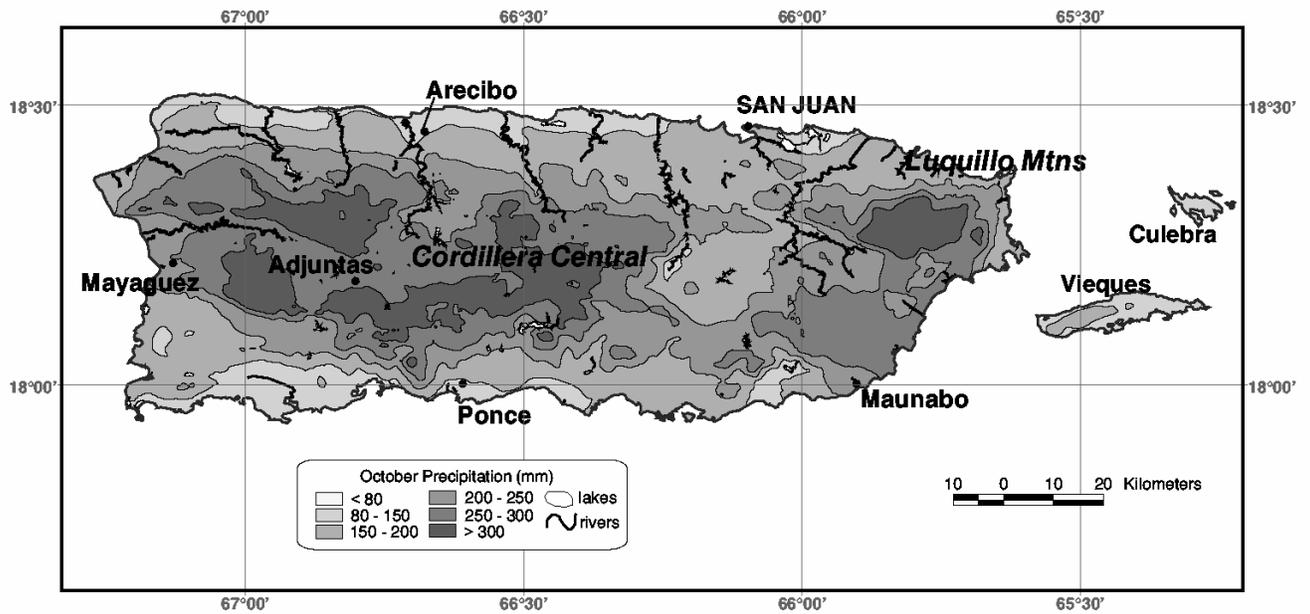
(a)

(b)

Figure 9. Mean 1963-95 precipitation in (a) January; (b) April for Puerto Rico, Vieques, and Culebra; PRISM parameterization

(c)

(d)

Figure 9 (Continued) Mean 1963-95 in (c) July; (d) October for Puerto Rico, Vieques, and Culebra; PRISM parameterization

Int. J. Climatol. 23: 1359-1381 (2003)

4. CONCLUSIONS

To support vegetation community and species distribution mapping, ecosystem modeling, and water resources management, PRISM climate mapping was performed on a monthly basis for mean daily maximum and minimum temperature and total precipitation for Puerto Rico, Vieques, and Culebra. PRISM was run under alternative parameterizations that simulated simpler interpolation methods as well as the full PRISM model. For temperature, the standard PRISM parameterization (PRISM), was compared to one in which the temperature/elevation slope was fixed at –6.5°C/km elevation (HYPS). For precipitation, the standard PRISM parameterization was compared to an inverse-distance weighting (IDW) interpolation. The effectiveness of each method was assessed, and compared and contrasted with other methods. Station data were summarized for the period 1963-1995, and interpolated to a regular grid with a resolution of 15 arc-seconds (~450 m). Input grids representing coastal influence, moisture availability, and atmospheric layer were developed to provide physically based guidance to the full PRISM model interpolation.

Spatial patterns in temperature were linked primarily to elevation, topographic position, and proximity to the ocean. Minimum and maximum temperature generally decreased with elevation, with the lowest temperatures occurring on the highest peaks of the Cordillera Central. Sheltered inland valleys in the vicinity of Adjuntas were characterized by low winter minimum temperatures of less than 13°C, which rivaled those on the higher peaks above. January minimum temperatures were warmest along the coastal strip (20-22°C), due to the moderating influence of the ocean. The mean layer 1 (boundary layer) regression slope for minimum temperature was lowest in winter (-3°C/km) and highest in summer (-4°C/km). Layer 2 (free atmosphere) slopes were more consistent throughout the year (-4.5 to -5°C/km). Maximum temperatures did not show an obvious coastal pattern, but did tend to be the warmest in areas receiving relatively little precipitation on an annual basis. In July, maximum temperatures ranged from about 32°C in the lowlands to about 25°C at the highest elevations. Maximum temperature slopes were steeper and relatively constant (-7 to -7.5°C/km) throughout the year.

In a cross-validation comparison with the full PRISM, the HPYS parameterization performed reasonably well for July maximum temperature. However, HYPS performed poorly for January minimum temperature, due primarily to lack of a spatially varying temperature/elevation slope, vertical atmospheric layer definition, and coastal proximity guidance. A comparison of the PRISM mean annual temperature map with a 1931-1960 map of mean annual temperature published by ESSA (1969a) showed a similar range of temperatures, but the ESSA map was much less detailed than the PRISM map.

Mean monthly precipitation varied significantly throughout the year, reflecting seasonally differing moisture trajectories. The winter months were the driest, and May and late summer and early fall were the wettest. Spatial precipitation patterns were associated most strongly with elevation, upslope exposure to predominant moisture-bearing winds, and proximity to the ocean. The Luquillo Mountains, in an exposed northeast location subject to strong orographic uplift, was by far the wettest region,
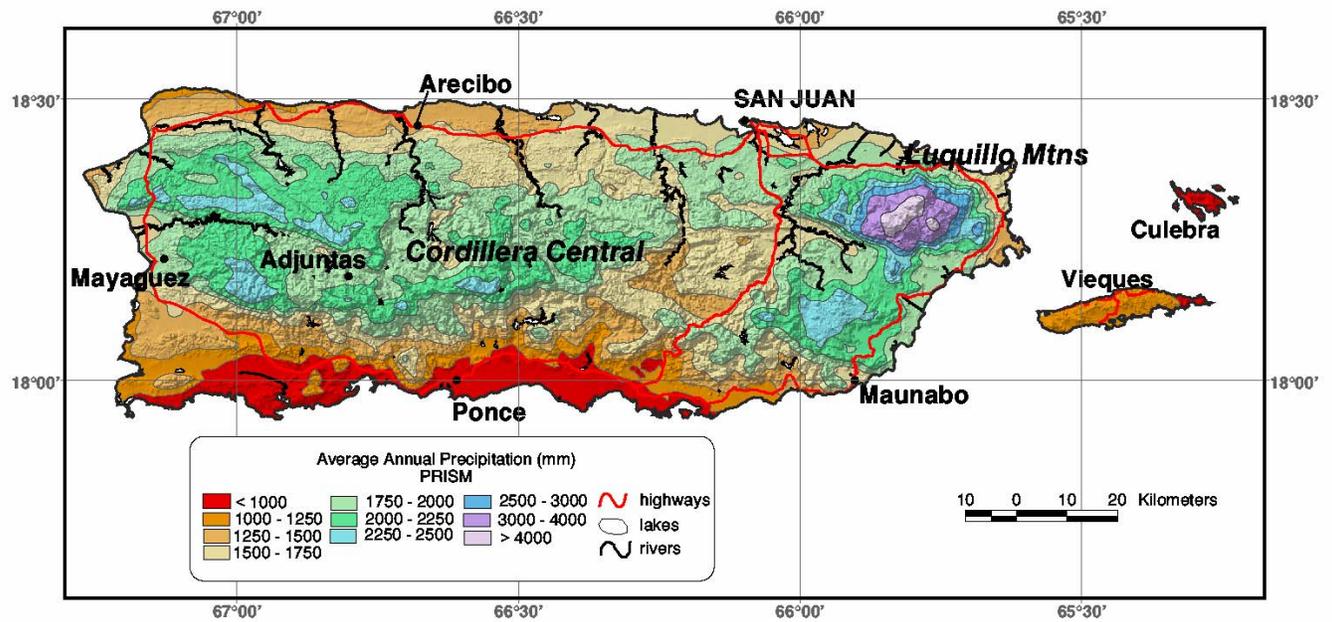
(a)
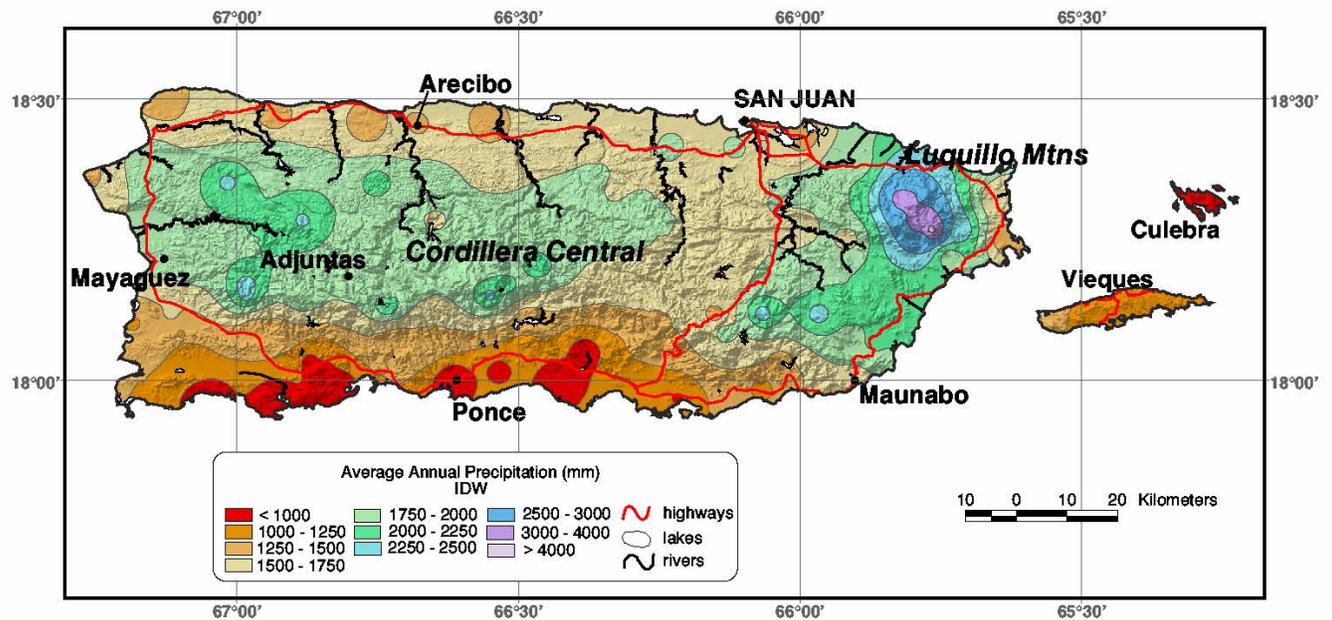
(b)

Figure 10. Mean 1963-95 annual precipitation for Puerto Rico, Vieques, and Culebra: (a) PRISM; (b) IDW

receiving up to 4500 mm annually. Secondary maxima of about 2500 mm occurred in the higher reaches of the Cordillera Central, the southeastern hills, and the western hills. The driest region was the south coast, where less than 850 mm per year was received. The rate of increase of precipitation with elevation was closely tied to the mean precipitation, and averaged 140% of the mean value per km.

Comparison of mean annual precipitation maps produced by the PRISM and IDW parameterizations showed similar broad-scale patterns, but significantly different details. Precipitation patterns produced by the IDW method were dictated by the values and locations of the data points, rather than the underlying topography or moisture regime. This produced a series of "bulls eyes" across the IDW map, with little recognizable structure. In contrast, the PRISM map showed no bulls eyes, but rather physically consistent patterns that followed elevation and moisture availability zones. IDW performed poorly in a cross-validation exercise compared to PRISM. This was due largely to the lack of elevation and moisture availability information in the interpolation process. Comparison of the PRISM annual precipitation map with a 1931-1960 map of mean annual precipitation published by ESSA (1969b) showed a similar range of values, but the ESSA map was less detailed than the PRISM map.

The application of the more sophisticated PRISM approach to mapping the climate of Puerto Rico, Vieques, and Culebra produced results that were superior to those of the simpler methods tested. The PRISM approach resulted in the greatest performance improvement for precipitation. The ability of PRISM to evaluate the relationships between precipitation and elevation was the most critical factor, with moisture availability guidance also being important. The PRISM approach also resulted in a large performance improvement for January minimum temperature. The ability of PRISM to divide the atmosphere into separate boundary and free atmospheric layers, evaluate rapidly varying temperature/elevation slopes, and access coastal proximity guidance, were all key factors. The PRISM approach resulted in a smaller performance improvement for July maximum temperature. Maximum temperature on Puerto Rico has a relatively stable temperature/elevation slope and minor coastal effects, so is more amenable to a fixed-slope approach.
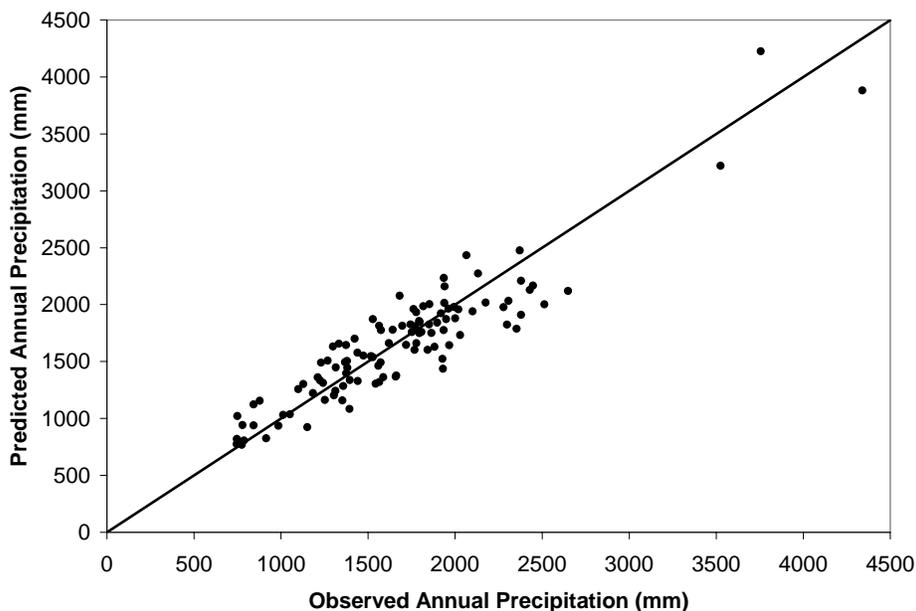
(a)

Figure 11. Scatterplots of predicted versus observed mean 1963-95 annual precipitation for Puerto Rico, Vieques, and Culebra: (a) PRISM
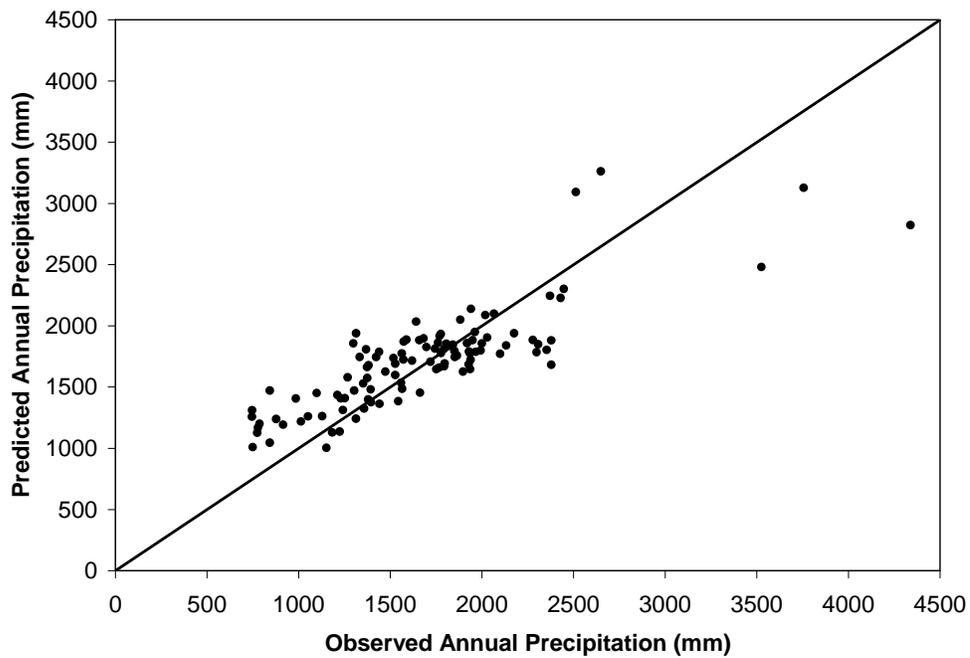
(b)

Figure 11. (Continued) Scatterplots of predicted versus observed mean 1963-95 annual precipitation for Puerto Rico, Vieques, and Culebra: (b) IDW
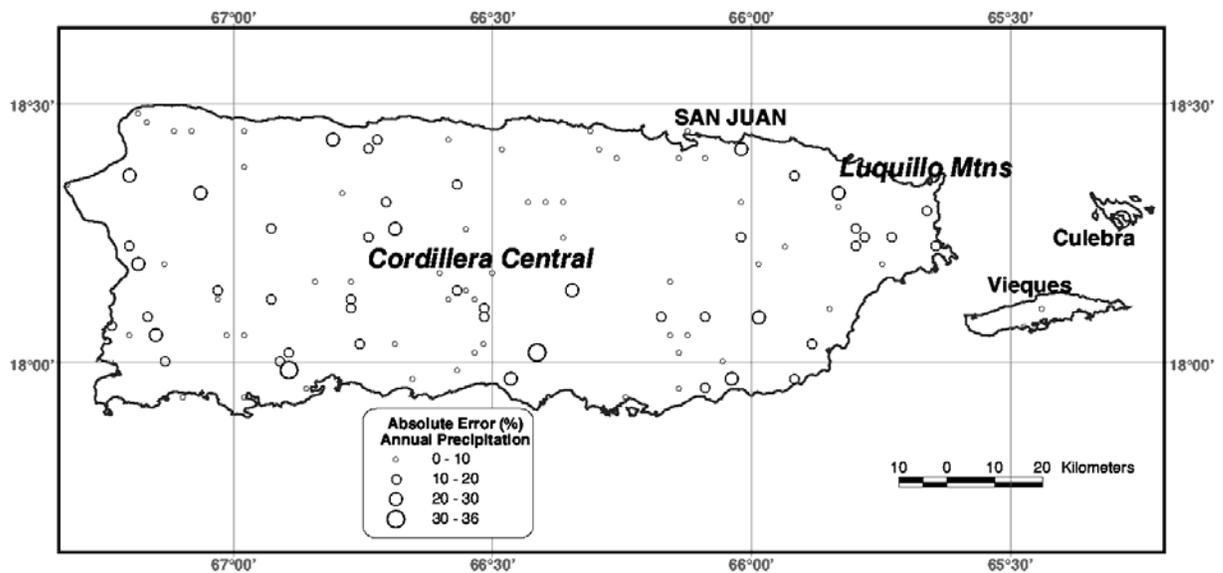

Figure 12. Cross-validation errors for mean 1963-95 annual precipitation for Puerto Rico, Vieques, and Culebra, PRISM parameterization.

LITERATURE CITED

Ahrens CD. *Meteorology Today: An Introduction to Weather, Climate, and the Environment*, 7th Edition. Pacific Grove, CA: Brooks-Cole – Thomson Learning, 544 pp.

Barnes SL. 1964. A technique for maximizing details in numerical weather map analysis. *J. Appl. Meteor.* **3**: 396-409.

Beard JS. 1949. Natural vegetation of the windward and leeward Islands. *Oxford Forestry Memoirs* **21**:1-192.

Bishop GD, Church MR, Daly C. 1998. Effects of improved precipitation estimates on automated runoff mapping: eastern United States. *J. Am. Water Resour. Assoc.* **34**: 159-166.

Bongers R, Poorter L, Van Rompaey RSAR, Parren MPE. 1999. Distribution of twelve moist canopy tree species in Liberia and Côte d'Ivore: response curves to a climatic gradient. *J. Veg. Sci.* **10**:371-382.

Burns JI. 1953. Small-scale topographic effects on precipitation distribution in San Dimas Experimental Forest. *Trans. Am. Geophys. Union* **34**:761-768.

Daly, C. 2002 (active April 2003). Variable influence of terrain on precipitation patterns: Delineation and use of effective terrain height in PRISM. http://www.ocs.orst.edu/prism/effter.pdf

Daly C, Gibson WP, Hannaway D, Taylor GH. 2000a. Development of new climate and plant adaptation maps for China. In: *Proc., 12th AMS Conf. on Applied Climatology, Amer. Meteorological Soc.*, Asheville, NC, May 8-11, J62-65.

Daly C, Gibson WP, Taylor GH, Johnson GL, Pasteris P. 2002. A knowledge-based approach to the statistical mapping of climate. *Clim. Res.*,22: 99-113.

Daly C, Johnson GL. 1999 (active April 2003). PRISM spatial climate layers: their development and use. *Short Course on Topics in Applied Climatology, 79th Annual Meeting of the American Meteorological Society*, 10-15 January, Dallas, TX. 49 pp. http://www.ocs.orst.edu/prism/prisguid.pdf

Daly C, Kittel TGF, McNab A, Gibson WP, Royle JA, Nychka D, Parzybok T, Rosenbloom N, Taylor GH. 2000b. Development of a 103-year high-resolution climate data set for the conterminous United States. In: *Proc., 12th AMS Conf. on Applied Climatology, Amer. Meteorological Soc.*, Asheville, NC, May 8-11, 249-252.

Daly C, Neilson RP. 1992. A digital topographic approach to modeling the distribution of precipitation in mountainous terrain. In: *Interdisciplinary Approaches in Hydrology and Hydrogeology, American Institute of Hydrology*, p 437-454.

Daly C, Nielson RP, Phillips DL. 1994. A statistical-topographic model for mapping climatological precipitation over mountainous terrain. *J. Appl. Meteorol*. **33**:140-158.

Daly C, Taylor GH, Gibson WP. 1997. The PRISM approach to mapping precipitation and temperature. In: *Proc 10th AMS Conf. on Applied Climatology, Amer. Meteorological Soc.*, Reno, NV, Oct 20-23, p 10-12.

Daly C, Taylor GH, Gibson WP, Parzybok TW, Johnson GL, Pasteris P. 2001. High-quality spatial climate data sets for the United States and beyond. *Transactions of the American Society of Agricultural Engineers* **43**: 1957-1962

ESSA. 1969a. Mean Annual Temperature Map for Puerto Rico. *U.S. Department of Commerce, Environmental Sciences Service Administration*.

ESSA. 1969b. Mean Annual Precipitation Map for Puerto Rico. *U.S. Department of Commerce, Environmental Sciences Service Administration*.

Ewel JJ, Whitmore JL. 1973. The ecological life zones of Puerto Rico and the U.S. Virgin Islands. USDA Forest Service Research Paper No. ITF-18, Institute of Tropical Forestry, Rio Piedras, PR. 72 p.

Foster DR, Motzkin G, Slater B. 1998. Land-use history as long-term broad-scale disturbance: regional forest dynamics and central New England. *Ecosystems* **1**: 96-119.

Garcia-Martinó AR, Warner GS, Scatena FN, Civco DL.1996a. Rainfall, runoff and elevation relationships in the Luquillo Mountains of Puerto Rico. *Carib. J. Sci*. **32**:413-424.

Garcia-Martino AR, Scatena FN, Warner GS, Civco DL. 1996b. Statistical low flow estimation using GIS analysis in humid montane regions in Puerto Rico. *J. Am. Water Resour. Assoc*. **32**(6):1259-1271.

Granger OE. 1983. The hydroclimatonomy of a developing tropical island -- a water resources perspective. *Annals of the Association of American Geographers* **73**:183-205.

He HS, Mladenoff DJ, Radeloff VC, Crow TR. 1998. Intergration of GIS data and classified satellite imagery for regional forest assessment. *Ecological Applications* **8**:1072-1083.

Helmer EH, Cohen WB, Brown S. 2000. Mapping montane tropical forest successional stage and land use with multi-date Landsat imagery. *International Journal of Remote Sensing* **21**:2163-2183.

Helmer, EH, Ramos, O, del Mar Lopez, T, Quiñones, M, Diaz, W. 2002. Mapping forest type and land cover of Puerto Rico, a component of the Caribbean biodiversity hotspot. *Caribbean Journal of Science* 38: 165-183.

Holdridge LR, Grenke WC, Hatheway WH, Liang T, Tosi JA. 1971. Forest environments in tropical life zones: a pilot study. *Pergamon Press*, New York, USA.

Host GE, Polzer PL, Mladenoff DJ, White MA, Crow TR. 1996. A quantitative approach to developing regional ecosystem classifications. *Ecol. Appl*. **6**:608-618.

Isaac C, Borque CPA. 2001. The ecological life zones of St. Lucia. *Global Ecol. Biogeogr*. **10**:549-566.

Iverson LR, Prasad AM. 1998. Predicting abundance of 80 tree species following climate change in the eastern United States. *Ecological Monographs* **68**:465-485.

Joseph L, Stockwell D. 2000. Temperature based models of the migration of Swainson's flycatcher *Myiarchus swainsoni* across South America: a new use for museum specimens of migratory birds. *Proceedings of the Academy of Natural Sciences*, 150:293-300.

Kyriakidis PC, Kim J, Miller N. 2001. Geostatistical mapping of precipitation from rain gauge data using atmospheric and terrain characteristics. *Journal of Applied Meteorology*, **40**:1855-1877.

Larsen M. 2001. Analysis of 20th-century rainfall and streamflow to characterize drought and water resources in Puerto Rico. In press, *Phys. Geog*. 22.

Legates DR, McCabe GJ. 1999. Evaluating the use of "goodness of fit" measures in hydrologic and hydroclimatic model validation. *Wat. Res. Res.* 35: 233-241.

Liu S, Reiners WA, Keller M, Schimel DS. 2000. Simulation of nitrous oxide and nitric oxide emissions from tropical primary forests in the Costa Rican Atlantic zone. *Environ. Model. Software* **15**:727-743.

López T del M., Aide TM, Scatena FN. 1998. The effect of land use on soil erosion in the Guadiana watershed in Puerto Rico. *Carib. J. Sci*. **34**:298-307. A

Lugo AE, Brown S, Dodson R, Smith TS, Shugart HH. 2000. The Holdridge life zones of the conterminous United States in relation to ecosystem mapping. *J. Biogeog.* **26**:1025-1038.

NCDC. 1995. Cooperative summary of the day, Volume 21, TD 3200 – Period of record through 1995. *National Climatic Data Center, National Oceanic and Atmonspheric Administration*, Asheville, NC. CD-ROM.

Neilson RP, Marks D. 1994. A global perspective of regional vegetation and hydrologic sensitivities from climate change. *J. Veg. Sci*. **5**:715-730.

Neilson RP. 1995. A model for predicting continental-scale vegetation distribution and water balance. *Ecol. Appl*. **5**: 362-385.

NOAA. 1974. Climates of the States, Vol. I – Eastern States. *U.S. Department of Commerce, National Oceanic and Atmospheric Administration*. 480 pp.

Ohmann JL, Spies TA. 1998. Regional gradient analysis and spatial pattern of woody plant communities of Oregon forests. *Ecol. Monogr*. 68, 151-182.

Ohmann JL, Gregory M. 2002. Predictive mapping of forest composition and structure with direct gradient analysis and nearest neighbor imputation in coastal Oregon, USA. *Can. J. For. Res*. In press.

Plantico M S, Goss LA, Daly C, Taylor GH. 2000. A new U.S. climate atlas. In: *Proc., 12th AMS Conf. on Applied Climatology, Amer. Meteorological Soc.*, Asheville, NC, May 8-11, 247-248.

Running SW, Gower ST. 1991. FOREST-BGC, a general model of forest ecosystem processes for regional applications II. Dynamic carbon allocation and nitrogen budgets. *Tree Phys*. **9**:147-160.

Running SW, Hunt Jr ER. 1993. Generalization of a forest ecosystem process model for other biomes, BIOME-BGC, and an application for global-scale models. Pp 141-158, IN: *Scaling Physiological Processes: Leaf to Globe*. J.R.Ehleringer and C.Field eds. Academic Press, London.

Scatena FN. 1998. An assessment of climate change in the Luquillo Mountains of Puerto Rico. Proceedings, tropical hydrology and Caribbean water resources, R.I.

Segarra-García, ed., *American Water Resources Association*, July 12-16, San Juan, Puerto Rico, p. 193-198.

Schermerhorn VP. 1967. Relations between topography and annual precipitation in western Oregon and Washington. *Wa.t Resour. Res.* **3**:707-711

Schwarb MC, Daly C, Frei C, Schar C. 2001a. Mean seasonal precipitation throughout the European Alps, 1971-1990. *Hydrologic Atlas of Switzerland*, National Hydrologic Service, Bern, Switzerland.

Schwarb MC, Daly C, Frei C, Schar C. 2001b. Mean annual precipitation throughout the European Alps, 1971-1990. *Hydrologic Atlas of Switzerland*, National Hydrologic Service, Bern, Switzerland.

Spreen WC. 1947. A determination of the effect of topography upon precipitation. *Trans. Am. Geophys. Union* **28**:285-290

Stockwell DRB, Peters D. 1999. The GARP Modeling System: problems and solutions to automated spatial prediction. *International Journal of Geographical Information Systems* **13**(2):143-158

Tian H, Melillo JM, Kicklighter DW, McGuire AD, Helfrich III J, Moore III B, Vörösmarty CJ. 2000. Climatic and biotic controls on annual carbon storage in Amazonian ecosystems. *Global Ecol. Biogeog.* **9**:315-335.

USDA-NRCS. 1998. PRISM Climate Mapping Project--Precipitation. Mean monthly and annual precipitation digital files for the continental U.S. *USDA Natural Resources Conservation Service, National Cartography and Geospatial Center*, Ft. Worth TX. December, CD-ROM.

Vogel RM, Wilson I, Daly C. 1999. Regional regression models of annual streamflow for the United States. *J. Irrigation and Drainage Engr.* **125**:148-157

*Wang H, Hall CAS, Scatena FN and Wu W. Spatial modeling of primary production and transpiration in the Luquillo Experimental Forest, Puerto Rico. In Review.

Willmott, CJ, Ackleson SG, Davis RE, Feddema JJ, Klink KM, Legates DR, O'Donnell J, Rowe CM. 1985. Statistics for the evaluation and comparison of models. *J. Geo. Res.*, 90: 8995-9005.

Woinarski JCZ, Fischer A, Milne D. 1999. Distribution patterns of vertebrates in relation to an extensive rainfall gradient and variation and soil texture in the tropical savannas of Northern Territory, Australia. *J. Trop. Ecol.* **15**:381-398.

*manuscripts in prep., in review, or in press.